ASSESSMENT OF SUBSURFACE STRATIGRAPHY USING 2-DIMENSIONAL ELECTRICAL RESISTIVITY IMAGING IN PART OF BENIN CITY, EDO STATE, NIGERIA.

BY

OMONUA, OSAVIE PRAISE

PSC1814528

DEPARTMENT OF PHYSICS

PHYSICAL SCIENCE

UNIVERSITY OF BENIN

BENIN CITY

JANUARY, 2025

ASSESSMENT OF SUBSURFACE STRATIGRAPHY USING 2-DIMENSIONAL ELECTRICAL RESISTIVITY IMAGING IN PART OF BENIN CITY, EDO STATE, NIGERIA.

BY

OMONUA, OSAVIE PRAISE

PSC1814528

A PROJECT WRITTEN AND SUBMITTED TO THE DEPARTMENT OF PHYSICS, FACULTY OF PHYSICAL SCIENCES, UNIVEERSITY OF BENIN IN PARTIAL FULFILLMENT OF THE REQUIREMENT OF BACHELOR OF SCIENCE (B.Sc.) IN APPLIED GEOPHYSICS OF THE UNIVERSITY OF BENIN,

BENIN CITY.

JANUARY, 2025

CERTIFICATION

We the undersigned, certify that OMONUA OSAVIE PRAISE of the Department of Physics, University of Benin, Benin City carried out this research work. The research has accordingly been accordingly been certified adequate in scope and quality for the partial fulfillment of the requirement for the award of B.Sc. in Physics.

_____ _____

PROF. C. O. AIGBOGUN **Date**

Supervisor

_____ _____

PROF. C. O. AIGBOGUN **Date**

Head of Physics Department

_____ _____

EXTERNAL EXAMINER **Date**

DEDICATION

I dedicate this work to Almighty God for the strength and ability to come this far and to finish well.

ACKNOWLEDGEMENT

First and foremost, I want to express my heartfelt gratitude to God Almighty for His constant guidance, strength, and blessings. I am especially grateful to my project supervisor, Prof. C. O. Aigbogun, whose guidance, patience, and encouragement have been instrumental in shaping this work. Your support has made this journey much smoother and more meaningful.

My special guidance and appreciation also goes the Head of Department of Physicss, Prof. C. O. Aigbogun, University of Benin (UNIBEN), and to all the lecturers in the Department of Physics for their commitment to academic excellence, encouragement, and dedication to imparting knowledge.

To my parents Mr & Mrs Omonua, thank you for your unwavering love, belief in me, and constant encouragement. I also want to acknowledge my wonderful siblings for your support and inspiration have been a source of strength throughout this process.

TABLE OF CONTENTS

LIST OF TABLE

LIST OF FIGURES

ABSTRACT

This study investigates the subsurface stratigraphy of Benin City, Edo State, Nigeria, using 2D Electrical Resistivity Imaging (ERI) techniques. The research aims to delineate geological formations, assess groundwater potential, and map subsurface layers critical for geotechnical and hydrogeological applications. Data were acquired along two traverses using the Wenner-Schlumberger array, revealing distinct layers with resistivity values ranging from 762 Ωm to 9940 Ωm, corresponding to topsoil, dry sand, and compact silty materials.

The analysis identified three subsurface layers, with depths extending to 54.3 meters and lateral extents up to 130 meters. Stratigraphic mapping provided detailed insights into the thickness, composition, and distribution of geological units. The results demonstrated a strong correlation between resistivity values and known geological formations, enabling the identification of aquifers and their potential water-bearing properties. These findings are crucial for urban planning, infrastructure development, and environmental management.

This study underscores the efficacy of ERI techniques in subsurface investigations, offering a reliable approach for mapping stratigraphy and evaluating groundwater resources. The integration of resistivity data with geotechnical insights provides a comprehensive framework for sustainable development in urban areas, ensuring better decision-making for future infrastructure and environmental projects.

CHAPTER ONE

INTRODUCTION

1.1 BACKGROUND OF STUDY

This research focuses on the vital role of subsurface stratigraphy, or subsurface characterization, in preventing the failure of buildings, bridges, and other structures. Inadequate understanding of the subsurface geological conditions, such as the geotechnical inadequacies of soil and the presence of geologic fissures beneath the construction site, has been identified as a primary cause of structural failures (Ilugbo et al., 2018b; Bawallah et al., 2019b; Bawallah et al., 2020; Oyedele et al., 2020). Thus, assessing the local bearing capacity and understanding the subsurface geological framework is crucial for the design and construction of stable, safe, and durable structures (Magawata et al., 2020).

Despite the known importance of pre-construction subsurface investigations, such as geophysical surveys, these essential steps are often overlooked or underutilized in the construction process due to cost constraints or a failure to integrate findings into the construction design and implementation phases (Ilugbo et al., 2018a; Adebiyi et al., 2018; Bawallah et al., 2019a). Recognizing the subsurface geology's significant impact on both the substructure and superstructure of buildings highlights the need for detailed subsurface characterization (Adebo et al., 2019; Aigbedion et al., 2019b).

Electrical Resistivity Tomography (ERT) has emerged as a key method in engineering geophysics for subsurface stratigraphy, offering detailed insights into the resistivity distribution, layer thickness, and depth across various subsurface layers. This technique is instrumental in identifying the complex geological features that may pose risks to structural integrity, such as faults, fractures,

and shear zones (Chambers et al., 2002; Kuras et al., 2008; Griffiths and Barker, 1993; Loke 2001; Andrews et al., 2013; Ugwu, 2012).

Nigeria's recent history of building collapses underscores the urgent need for comprehensive subsurface characterization before construction. Many of these incidents could be attributed to buildings erected on soils with inadequate bearing capacity, without prior geophysical investigations that could have revealed the unsuitability of the subsurface conditions (Sands, 2002). Subsurface characterization can identify potential challenges such as expansive clays, shallow bedrock, or high water tables, which are critical for ensuring the stability and safety of structures.

This study employs Electrical Resistivity Tomography to investigate the subsurface stratigraphy of a section of the University of Benin Teaching Hospital (Golf Course Area), aiming to delineate aquiferous zones and provide detailed geophysical and geological information about the subsurface structures. Previous studies in various parts of Nigeria, including Edo State, have demonstrated the effectiveness of the electrical resistivity method in subsurface characterization for a range of applications, from aquifer identification to the construction of subsurface geological maps (Ezomo et al., 2009; Alile et al., 2008; Alile et al., 2011; Abdulahi et al., 2011; Aigbogun and Egbai, 2012). This research contributes to the broader field of geotechnical engineering by highlighting the importance of subsurface stratigraphy in mitigating the risk of structural failures and ensuring the long-term stability and safety of constructed facilities.

1.2 SUBSURFACE STRATIGRAPHY

Subsurface stratigraphy encompasses the study of the arrangement, composition, and properties of geological layers beneath the Earth's surface. These layers, formed over millions of years through various geological processes, hold valuable information about the Earth's history, geological

events, and resource distribution. Understanding subsurface stratigraphy is vital for a wide range of applications, spanning from engineering and environmental assessments to resource exploration and management.

1.2.1 Components of Subsurface Stratigraphy

Formation and Deposition: Subsurface stratigraphy involves the analysis of sedimentary formations and their depositional environments. Sedimentary rocks, such as sandstone, shale, and limestone, record information about past environments, including ancient oceans, lakes, rivers, and deserts. By studying the characteristics of sedimentary layers, geoscientists can reconstruct the depositional history of an area and infer past environmental conditions.

1. Sequence Stratigraphy

Sequence stratigraphy is a conceptual framework used to interpret the stacking patterns of sedimentary layers and their relationships to sea-level changes and basin evolution. It involves identifying repetitive cycles of sedimentation, known as depositional sequences, which reflect changes in sea level and sediment supply over time. Sequence stratigraphy helps geoscientists correlate rock units, understand basin evolution, and predict the distribution of reservoirs and source rocks in subsurface environments.

2. Fossil Assemblages

Fossils preserved within sedimentary rocks provide valuable information about past life forms, environmental conditions, and the age of rock formations. By studying fossil assemblages, paleontologists can reconstruct past ecosystems, track evolutionary changes, and establish the relative ages of sedimentary layers through biostratigraphy.

3. Structural Geology

Subsurface stratigraphy is closely linked to structural geology, the study of the deformation and geometry of rock layers due to tectonic forces. Structural features such as faults, folds, and fractures influence the distribution and orientation of sedimentary layers, affecting their thickness, dip, and lateral continuity. Understanding the structural architecture of subsurface strata is essential for interpreting geological maps, predicting seismic hazards, and assessing reservoir quality in hydrocarbon exploration.

1.2.2. Importance of Subsurface Stratigraphy Assessment

1. Engineering Applications

Subsurface stratigraphy assessment is crucial for engineering projects such as building construction, infrastructure development, and land use planning. It provides insights into the geological conditions underlying a site, influencing decisions related to construction design, foundation stability, and risk assessment for natural hazards such as landslides and subsidence.

2. Environmental Assessment

Subsurface stratigraphy assessment plays a fundamental role in environmental assessments by helping to identify potential contamination pathways, assess groundwater flow dynamics, and predict the movement of pollutants. This information is critical for conducting environmental impact assessments, designing remediation strategies, and safeguarding groundwater resources.

3. Resource Exploration

Understanding subsurface stratigraphy is essential for resource exploration endeavors, including the search for minerals, groundwater, and hydrocarbons. By characterizing subsurface geological layers, geoscientists can identify potential resource-bearing formations, predict their distribution and quality, and guide exploration efforts to maximize resource recovery.

4. Hydrocarbon Exploration

Subsurface stratigraphy plays a central role in hydrocarbon exploration and production. By analyzing the distribution, geometry, and quality of sedimentary reservoirs and source rocks, geoscientists can identify potential hydrocarbon-bearing formations, assess reservoir connectivity and productivity, and optimize drilling and production strategies.

5. Groundwater Resource Assessment

Understanding subsurface stratigraphy is critical for assessing groundwater resources and aquifer properties. By characterizing the lithology, porosity, and permeability of subsurface formations, hydrogeologists can delineate aquifer systems, predict groundwater flow patterns, and develop sustainable water management strategies for drinking water supply, irrigation, and environmental conservation.

Geophysics involves the use of non-invasive techniques to determine subsurface anomalies without having to engage in destructive excavation (Barker, 1993). Non-destructive testing (NDT) is defined as the evaluation of the properties of a material, component or system without causing damage (Louis, 1995). In the last few decades, geophysical NDT methods have been developed and increasingly applied for addressing engineering problems. As one example, transportation personnel have used geophysical NDT methods in assisting geotechnical site investigation, construction, and maintenance of highways (Dahlin, 2001; Wightman and Jalinoos, 2003). In many instances, geophysical NDT methods enhance the reliability and speed, and also reduce the cost of a geotechnical investigation (Anderson et al., 2008). Assessing and characterizing geotechnical conditions can become complex and costly in the presence of obstacles such as difficult access, irregular terrain and ground conditions, or regulatory constraints. Results based on traditional methods such as penetration testing or direct sampling may be of limited utility.

Surface geophysical techniques can provide alternate, wide-area methods for subsurface characterization and information regarding relevant material properties (Rucker, 2006). Though geophysics is not a substitute for geotechnical boring or testing, it is often a very cost-effective and efficient means of constructing contiguous 2D and 3D images of the subsurface and determining in-situ bulk properties (Anderson et al., 2008). Geophysics involves the use of non-invasive techniques to determine subsurface anomalies without having to engage in destructive excavation (Barker, 1993). Non-destructive testing (NDT) is defined as the evaluation of the properties of a material, component or system without causing damage (Louis, 1995). In the last few decades, geophysical NDT methods have been developed and increasingly applied for addressing engineering problems. As one example, transportation personnel have used geophysical NDT methods in assisting geotechnical site investigation, construction, and maintenance of highways (Dahlin, 2001; Wightman and Jalinoos, 2003). In many instances, geophysical NDT methods enhance the reliability and speed, and also reduce the cost of a geotechnical investigation (Anderson et al., 2008).

Assessing and characterizing geotechnical conditions can become complex and costly in the presence of obstacles such as difficult access, irregular terrain and ground conditions, or regulatory constraints. Results based on traditional methods such as penetration testing or direct sampling may be of limited utility. Surface geophysical techniques can provide alternate, wide-area methods for subsurface characterization and information regarding relevant material properties (Rucker, 2006). Though geophysics is not a substitute for geotechnical boring or testing, it is often a very cost-effective and efficient means of constructing contiguous 2D and 3D images of the subsurface and determining in-situ bulk properties (Anderson et al., 2008).

1.3 APPLICATION OF ELECTRICAL RESISTIVITY TOMOGRAPHY (ERT)

Geophysics involves the use of non-invasive techniques to determine subsurface anomalies without having to engage in destructive excavation (Barker, 1993). Non-destructive testing (NDT) is defined as the evaluation of the properties of a material, component or system without causing damage (Louis, 1995). In the last few decades, geophysical NDT methods have been developed and increasingly applied for addressing engineering problems. As one example, transportation personnel have used geophysical NDT methods in assisting geotechnical site investigation, construction, and maintenance of highways (Dahlin, 2001; Wightman and Jalinoos, 2003). In many instances, geophysical NDT methods enhance the reliability and speed, and also reduce the cost of a geotechnical investigation (Anderson et al., 2008). Assessing and characterizing geotechnical conditions can become complex and costly in the presence of obstacles such as difficult access, irregular terrain and ground conditions, or regulatory constraints. Results based on traditional methods such as penetration testing or direct sampling may be of limited utility. Surface geophysical techniques can provide alternate, wide-area methods for subsurface characterization and information regarding relevant material properties (Rucker, 2006). Though geophysics is not a substitute for geotechnical boring or testing, it is often a very cost-effective and efficient means of constructing contiguous 2D and 3D images of the subsurface and determining in-situ bulk properties (Anderson et al., 2008).

The electrical resistivity tomography (ERT) method is one of the most widely used near-surface geophysical survey methods for civil engineering applications (Castilho and Maia, 2008). The method has been used for mapping electrical resistivity in two and three dimensions (Dahlin, 2001). Previous studies have demonstrated the use of the ERT method for identification of bedrock structures (Hsu et al., 2010; Chambers et al., 2013), cavities or sinkholes (Kaufmann et al., 2012;

Gómez-Ortiz and Martín-Crespo, 2012), geotechnical site investigation (Al-Fares W., 2011; Haile and Atsbaha, 2014), slope stability investigation (Marescot et al., 2008; Perrone et al., 2014), and unknown bridge foundation determination (Arjwech et al., 2013; Tucker et al., 2014). The ERT method may be used for various other purposes in subsurface engineering investigations. This paper aims to further demonstrate the application of the ERT technique on a number of engineering problems. More specifically, the paper presents the results of 2D ERT that have been carried out by the authors in various projects including investigating the subsurface geology of a building construction site, determining the depth of an unknown bridge foundation, and determining seepage from the earthen embankments of a wastewater treatment pond system.

1.4 ELECTRICAL RESISTIVITY SURVEY

The electrical resistivity technique is based on the assumption that subsurface geological materials exhibit a wide variability of resistivity values and that geological boundaries can be identified based on measurements of resistivity. If a target of interest has a sufficiently large electrical resistivity contrast with respect to that of the surrounding material, it can be detected by surface measurements of voltage following the injection of current through pairs of electrodes (Barker, 1993). The purpose of a resistivity survey is thus to determine the distribution of underground resistivity from measurements of potential difference, or voltage, made on the ground surface. An electric current I (amperes, A) is injected at electrode C_1 and withdrawn at electrode C_2 as shown in Figure 1.1, while two other electrodes P_1 and P_2 are used to record the resulting potential difference ÄV (volt, V),

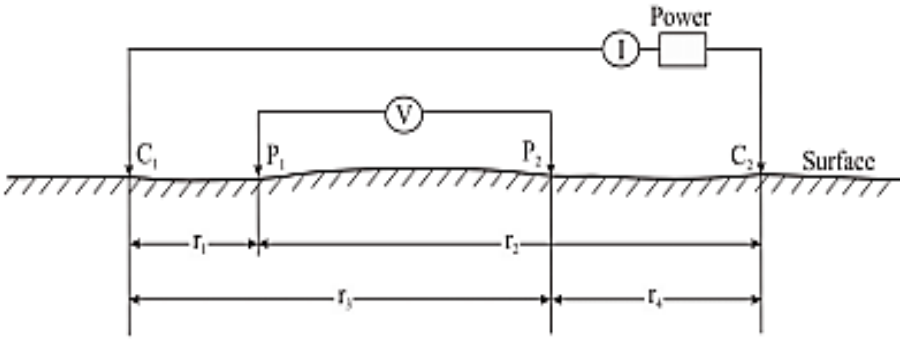

Figure 1.1: Two current (C_1 and C_2) and two potential (P1 and P_2) electrodes in the standard configuration (Telford et al., 1990).

$$\Delta V = \frac{I\rho}{2\pi}\left\{\left(\frac{1}{r_1}-\frac{1}{r_2}\right)-\left(\frac{1}{r_3}-\frac{1}{r_4}\right)\right\} \quad (1.1)$$

Where r is resistivity, while r_1 , r_2, r_3, and r_4 are distances of the potential electrodes P_1 and P_2 from the current electrodes C_1 and C_2 , respectively. Equation 1.1 is valid if the ground has homogeneous resistivity. In case of inhomogeneous ground, an apparent resistivity r, a is calculated from the relationship between the applied current and the potential difference for a particular electrode arrangement and spacing. It is defined by,

$$\rho_a = K\frac{\Delta V}{I} \quad (1.2)$$

Where k is a geometric factor dependent on the electrode spacing,

$$K = \frac{2\pi}{\left\{\left(\frac{1}{r_1}-\frac{1}{r_2}\right)-\left(\frac{1}{r_3}-\frac{1}{r_4}\right)\right\}} \quad (1.3)$$

The apparent resistivity clearly depends on the geometry of the electrode configuration. The best electrode configuration for a field survey depends on the sensitivity of the resistivity meter, the background noise level, and the relative importance assigned by the geophysicist to depth of

penetration and lateral resolution. Standard electrode configurations used for 2D ERT surveys are Wenner, dipoledipole, Wenner-Schlumberger, pole-pole, pole-dipole, and equatorial dipole-dipole (Telford et al., 1990; Loke, 2000; Kearey and Brooks, 2002; Dahlin and Zhou, 2004; Loke and Lane, 2004; Loke, 2010).

1.4.1 1D Resistivity Surveying – Applications, Limitations and Pitfalls

Generally, there are two possible methods for 1-D resistivity surveying. They are the vertical electrical sounding (drilling) and horizontal profiling (electrical mapping or trenching) methods.

1. Vertical Electrical Sounding (drilling)

In this method, the center point of the electrode array remains fixed, but the spacing between the electrodes is increased to obtain more information about the deeper sections of the subsurface. The measured apparent resistivity values are normally plotted on a log-log graph paper. To interpret the data from such a survey, it is normally assumed that the subsurface consists of horizontal layers. The basis for making an electrical sounding irrespective of the electrical array used is the fact that the farther away from a current source the measurement of the potential is, the deeper the probing will be. Hence it primarily provides information about the variation of electrical resistivity with depth. This method has given useful results for geological situations (such the water-table) where the one-dimensional model is approximately true. The greatest limitation of the resistivity sounding method is that it does not take into account lateral changes in the layer resistivity. The failure to include the effect of such lateral changes can results in errors in the interpreted layer resistivity and/or thickness.

2. Horizontal Profiling (electrical mapping or trenching)

This is another classical electrical resistivity surveying technique. In this case, the spacing between the electrodes remains fixed, but the entire array is moved along a straight line. Maximum apparent

resistivity anomalies are obtained by orienting the profiles at right angle to the strike of the geologic structure. This gives some information about lateral changes in the subsurface resistivity, but it cannot detect vertical changes in the resistivity. In order to make amends for this inadequacy, it is recommended that at least two different electrode spacing be used. This will aid in distinguishing the effects of shallow geologic structures from the effects of deeper ones. This is because the effect of shallow geologic features is suppressed in the profile made with larger spacings, whereas the effect of deeper features is retained. However, the depth of investigation is still very much limited. Interpretation of data from profiling surveys is mainly qualitative.

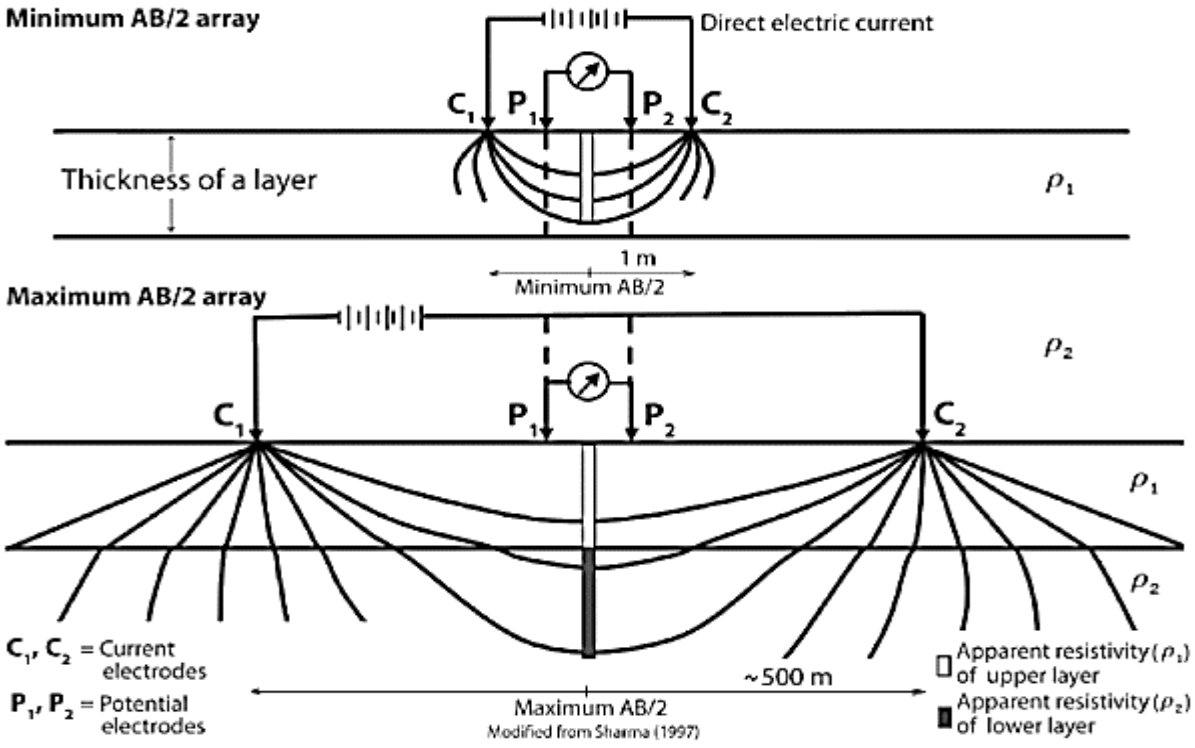

Figure 1.2: Schlumberger array and 1D resistivity model output (modified from Sharma, 1997).

In many engineering and environmental studies, the subsurface geology is very complex where the resistivity can change rapidly over short distances. The 1- D resistivity sounding method might

not be sufficiently accurate for such situations. To obtain a more accurate subsurface model than is possible with a simple 1-D model, a more complex model must be used. In a 2-D model, the resistivity variations in two directions are obtained. A more realistic model would be a fully 3-D model where the resistivity values are allowed to change in all 3 directions.

1.4.2 2D Electrical Resistivity Tomography

A 2D multi-electrode ERT survey may be carried out using a large number of electrodes connected to a multi-core cable. The electrode cable is typically divided into sections of manageable length, which are then connected end-to-end. Electrodes connected to the cable take-outs are inserted into the ground at a specified regular interval along a survey line. A resistivity meter and electronic switching unit are used in conjunction with a user-programmed protocol to automatically measure r/a in a pre-defined sequence of combinations of four electrodes. Efficient data acquisition is achieved by measuring several voltages simultaneously across multiple pairs of electrodes following a single injection of electric current (Loke, 2000; Bernard, 2003; Hiltunen and Roth, 2003; Loke, 2010). Figure 1.2 shows an example of electrode arrangement and measurement sequence for a 2D ERT survey. When the data acquisition is completed, data analysis is performed using the RES2DINV (Loke, 2004) software, including 2D pseudo-section plotting, and inversion. The RES2DINV inversion algorithm is described by Loke and Barker (1995; 1996) and Yang (1999) and is based on a smoothnessconstrained least squares approach (DeGroot-Hedlin and Constable, 1990).

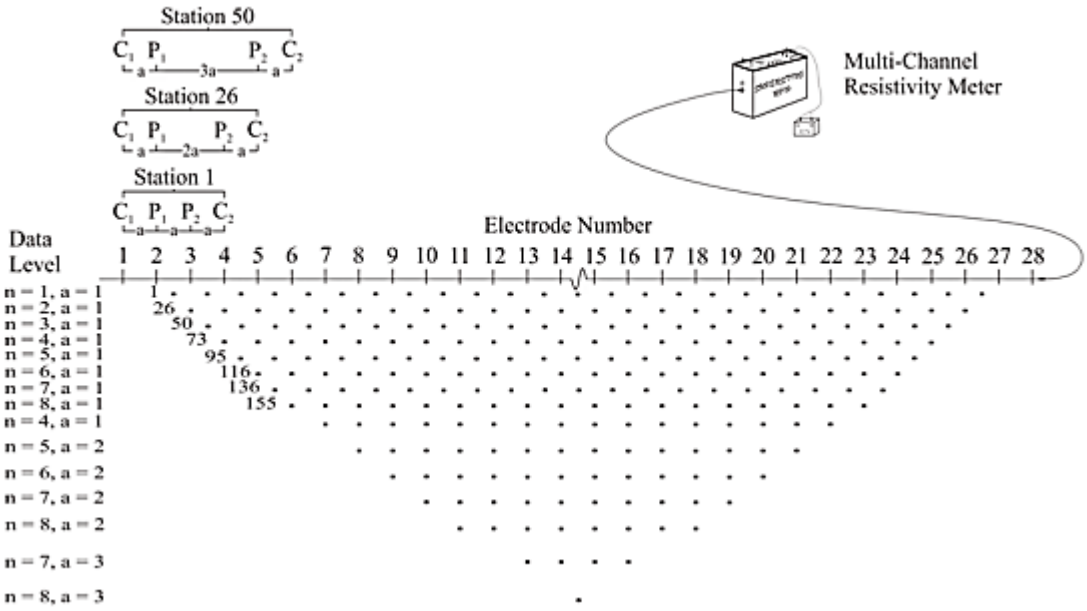

Figure 1.3: Arrangement of electrodes for a 2D survey and the sequence of measurements used to build up an apparent resistivity pseudo-section (Loke, 2000).

1.5 PITFALLS IN 2-D RESISTIVITY SURVEYS AND INVERSION

While 2-D resistivity surveys have made the mapping of many complex structures possible, caution must still be exercised in interpreting the results from the data. Below are some of the common pitfalls.

(a) Incorrect use of the dipole-dipole array

This is still a surprisingly common problem.

There are two common mistakes in the use of this array. The first is to assume that the depth of investigation is at the point of intersection of the two 45° diagonals projected from the dipoles. This greatly overestimates the depth of investigation. The second common mistake is to monotonically increase the “n” factor, while keeping the dipole length “a” fixed, in an effort to increase the depth of investigation. This usually results in very noisy and unusable data, with

negative apparent resistivity values in some cases, for “n” values of greater than 8. To solve this problem the “n” value should not exceed 6, and the method of overlapping data levels with different “a” dipole lengths can be used.

(b) Mistakes in the field

This can arise from a variety of sources. It could be caused by instrumentation errors during the field survey, poor electrode contact in dry, sandy or stony ground, shorting of electrodes due to very wet conditions or metal objects (such as fences, pipes etc.) or mistakes such as attaching electrodes to the wrong connectors.

(c) 3-D geology

It is assumed that the subsurface is 2-D when interpreting the data from a single line. This assumption is valid if the survey is carried out across the strike of an elongated structure. If there are significant variations in the subsurface resistivity in a direction perpendicular to the survey line (i.e. the geology is 3-D), this could cause distortions in the lower sections of the model obtained. Measurements made with the larger electrode spacings are not only affected by the deeper sections of the subsurface, they are also affected by structures at a larger horizontal distance from the survey line. This effect is most pronounced when the survey line is placed near a steep contact with the line parallel to the contact. Dahlin and Loke (1997) did a comparison of the sensitivity of different arrays to structures off the axis of a 2-D survey line. In general, it was found that the dipole-dipole array was the most sensitive (i.e. suffered the greatest distortion) due to off-axis structures. The best way to handle 3-D structures would be a full 3-D survey and data inversion. It must be emphasized that a 2-D survey with very good quality data and very dense data coverage, and inverted with a good inversion algorithm, can still give the wrong results if the assumption of a 2-D geology on which the model is based is seriously wrong. This is a particularly

a problem in mineral surveys (which commonly also involve IP measurements) where very complex geological structures and mineralization patterns are usually encountered. In such situations, the results from a 2-D resistivity and IP model should be treated with some reservations unless it is confirmed by a 3-D survey and model. There have been many cases where expensive drill-holes have passed through barren zones in areas where the 2-D model shows a strong IP anomaly.

(d) Limits of the physics of the resistivity method

While 2-D and 3-D surveys and data inversion has greatly extended the range of field problems that can be solved using the resistivity method, there are still basic laws of physics that place certain limitations on these techniques. The resolution of the resistivity method decreases exponentially with depth. We see the subsurface "as through a glass darkly" and the image becomes increasingly fuzzier with depth. It is unlikely to be able to map a structure with a size of 1 meter at a depth of 10 meters using the resistivity method. The resistivity phenomenon is based on the diffusion equations, so its resolution is inherently poorer than the seismic or ground radar method at depths greater than one wavelength.

(e) Non-uniqueness

It is well known that more than one model can produce the same response that agrees with the observed data within the limits of the data accuracy. In 1-D resistivity sounding modeling, the problems of equivalence and suppression are well known. The problems, in different forms, also occur in 2-D and 3-D modeling. A good example was shown in the paper by Oldenburg and Li (1999). In 2-D and 3-D modeling, constrains are used so that a stable solution can be obtained. The use of a smooth or blocky constrain results in the production of models that look more reasonable, but it is no guarantee that they are indeed correct. The accuracy of the result is

only as good as the accuracy of the assumptions made. The resulting model thus depends to a significant extent on the constrain used, and will closely approximate the true subsurface resistivity only if the constrains correspond to the real situation.

(f) Optimization versus inversion

The RES2DINV program, like most non-linear inversion programs, actually carries out an optimization (i.e. not a direct one-to-one inversion in the sense it must have only one solution) in that it tries to reduce the difference between the calculated and measured apparent resistivity values. If there is infinite data and a perfect fit between the calculated and measured values, how the data is measured should not have an effect on the results. However with real, noisy and limited data, how the data is measured does have an effect. A model with 5% rms error in the fit between the measured and calculated apparent resistivity values with one data set might not give the same model as a 5% rms error with another data set although both might be from the same place. For this reason, the dipole-dipole array gives an inversion model with much better resolution than the pole-pole array although in theory the dipole-dipole values can be extracted from the pole-pole values.

(g) Increasing the electrode separation does not always increase the survey depth

It is generally assumed that as the separation between the electrodes is increased, the region of the subsurface that is 'sensed' by the array also increases. While this is true of most arrays, there are certain important exceptions. In particular, this is not true of the pole-dipole and dipole-dipole arrays under certain circumstances. In some surveys with the pole-dipole array, the separation between the C1 current electrode and the P1-P2 dipole is increased in an effort to increase the depth of survey by the array. However, if this is done with the P1-P2 dipole length kept at a constant spacing, certain interesting effects come into play. This problem can be overcome by a

combination of using higher currents and more sensitive receivers. However, the problem caused by the change in the array sensitivity pattern as the 'n' factor is monotonically increased is usually not taken into account. Thus increasing the separation between the current electrode and the potential dipole, while keeping the dipole length fixed, does not increase the survey depth of the array. It, in fact, effectively decreases the depth of the region sensed by the array!

Note that the amplitude of the high resistivity anomaly due to the near-surface block increases with the 'n' value, i.e. the array becomes increasingly more sensitive to the near-surface block as the separation between the electrodes increase. In field surveys with the pole-dipole array where the 'n' factor is monotonically increased in the belief that this increases the survey depth, the pseudosection is frequently dominated by a series of parallel slanting high-amplitude anomalies due to near-surface in homogeneities. The anomalies due to the near-surface structures frequently mask the anomalies due to deeper structures that are of interest.

1.5.1 Sources of Noise in Electrical Resistivity Data Acquisition

Discussed briefly below, are a number of noise sources that can affect our measurements of voltage and current from which we desire to compute apparent resistivities.

1. Electrode Polarization: A metallic electrode, like a copper or steel rod, in contact with an electrolyte other than a saturated solution of one of its own salts, like ground water, will generate a measurable contact potential. In applications such as SP, these contact potentials can be larger than the natural potential that you are trying to record. Even for the DC methods, these potentials can be a significant fraction of the total potential measured. For DC work, there are two possible solutions.

a. Use nonpolarizing electrodes. These are electrodes that contain a metallic conducting rod in contact with a saturated solution of its own salt. Copper and copper sulfate solutions are commonly

used. The rod and solution are placed in a porous ceramic container that allows the saturated solution to slowly leak out and make contact with the ground. Because these solutions are rather environmentally unfriendly these porous pot electrodes are rarely used in DC work. They are, however, commonly used in SP and IP surveys.

b. A simple method to avoid the influence of these contact potentials is to periodically reverse the current flow in the current electrodes or use a slowly varying, a few cycles per second, AC current. As the current reverses, the polarizations at each electrode break down and begin to reverse. By measuring over several cycles, robust current and voltage measurements can be made with negligible polarization effects.

2. Telluric Currents: As described previously, naturally existing currents flow within the earth. These currents are referred to as telluric currents. The existence of these currents can generate a measurable voltage across the potential electrodes even when no current is flowing through the current electrodes. By periodically reversing the current from the current electrodes, or by employing a slowly varying AC current, the effects of telluric currents on the measured voltage can be cancelled.

3. Presence of Nearby Conductors: Electrical surveys cannot be performed around conductors that make contact with the ground. For example, the presence of buried pipes or chain-linked fences will act as current sinks. Because of their low resistivity, current will preferentially flow along these structures rather than flowing through the earth. The presence of these nearby conductors essentially acts as electrical shorts in the system.

4. Low Resistivity at the Near Surface: Just as nearby conductors can act as current sinks that short out an electrical resistivity experiment, if the very near surface has a low resistivity, it is

difficult to get current to flow more deeply within the earth. Thus, a highly conductive near-surface layer such as a perched water table can prevent current from flowing more deeply within the earth.

5. Near-Electrode Geology and Topography: Any variations in geology or water content localized around an electrode that produce near-surface variations in resistivity can greatly influence resistivity measurements. In addition, rugged topography will act to concentrate current flow in valleys and disperse current flow on hills.

6. Not letting the current charge decay: When an electrode is used as a current electrode, charges tend to build up around the electrode. When the current is no longer flowing through the electrode, it still takes a finite amount of time for the charges to disperse. If the same electrode is used as a potential electrode immediately after it has been used as a current electrode, this could result in an erroneous reading (Dahlin 2000).

7. Current Induction in Measurement Cables: Current flowing through the cables connecting the current source to the current electrodes can produce an induced current in the cables connecting the voltmeter to the voltage electrodes, thereby generating a spurious voltage reading. This source of noise can be minimized by keeping the current cables physically away from, a meter or two, the voltage cables.

8. Instrumental noise: Also referred to as systematic noise, these are caused by faults in the instruments used. They can be reduced by improving on the quality of the instrument used for the survey.

9. Long linear features: These may be in the form of rivers, wires or more generally, small subsurface conducting bodies which may channel the current far away from the area of interest and as such result in current leakage.

1.5.2 Methods of improving signal to noise ratio

The most effective method of improving signal/noise ratio is to increase the signal strength. Modern instruments often provide observers with direct readings of $\frac{V}{I}$, measured in ohms, and so tend to conceal voltage magnitudes. Small ohm values indicate small voltages but current levels also have to be taken into account. There are physical limits to the amount of current any given instrument can supply to the ground and it may be necessary to choose arrays that give large voltages for a given current flow, as determined by the geometric factor. The Wenner and two-electrode arrays score more highly in this respect than most other arrays.

1.6 STUDY AREA

The site chosen for this study is the Benin City Metropolis. The Benin Metropolis comprises of 7 Local Government areas out of the 18 LGA in Edo State. These 7 local Government area makes up more than half of the entire population of the state. The study location chosen for this study was the 4 most densely populated in Benin Metropolis which lies between latitudes N6^{o}30’43.2’’ *to N6^{o}14’ 50.8’’ and longitudes E5^{o}33’58.6’’ to E5^{o}50’ 02.1’’.*

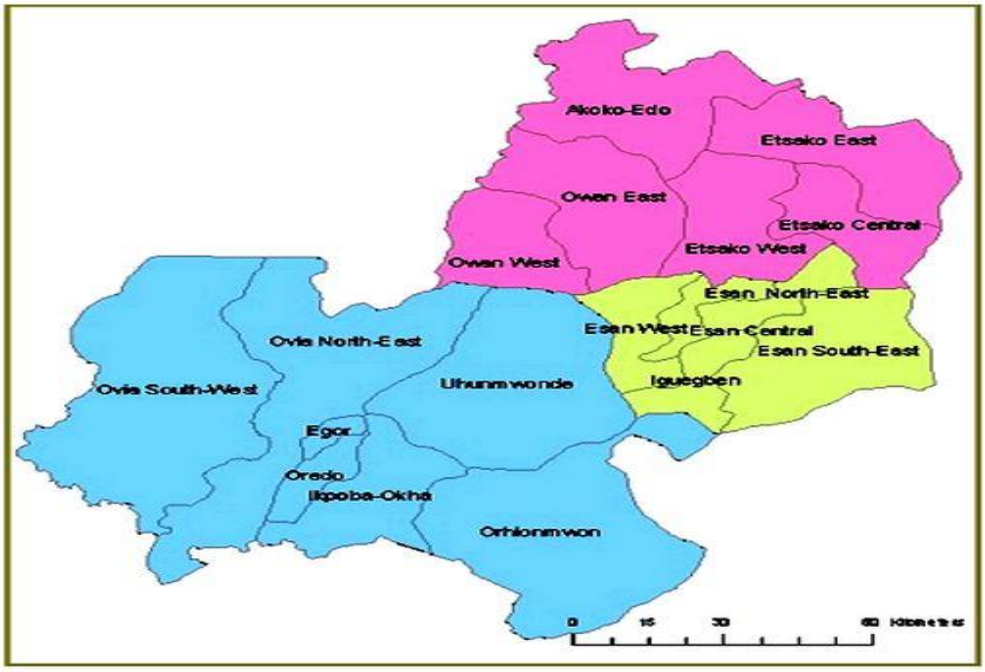

Figure 1.4: Map of Edo State showing the 18 Local Governments

1.7 GEOGRAPHICAL SETTING

1.7.1 Climate

Benin City has two seasons, the wet and the dry seasons. The wet season last from March to October while the dry season is from November to February with scanty rainfall. These seasons are controlled by the position of the Inter-Tropical Discontinuities (ITD) whose movement is reflected in the corresponding shifts with the rain belt (Aziegbe, 2000). The wet season begins in March and reaches its first maximum in July and the second is September. Both maxima are separated by a brief spell referred to as “August Break”. In any case, rainfall is experienced throughout the year with December and January being the driest. The tropical maritime air mass and the tropical continental air mass are the prevailing winds in the area. The maritime air mass

dominates the area through a greater part of the year. The monthly rainfall in Benin is higher in the months of May, June, July, September and October (Eseigbe and Oisasoje, 2012).

1.7.2 Topography

Benin City is about 85m above the sea level at the highest point. Sixty (60) flood sites and 25 erosion sites are within Benin metropolis (Odjugo and Iweka, 2006). While some of these are still minor environmental problems, others are major and devastating. Some of the worst erosion sites in Benin City as indicated by the Ministry of Environment, Edo State include the University of Benin and Ogbesan quarters.

Benin City is built on a nearly undulating low-lying surface. The eastern edge of it is tilted towards the Ikpoba River that drains the eastern portion of the city while the Western edge slopes gently towards Ogba stream that drains the Western portion of the City. Benin City is drained by a series of entrenched river and small streams such as Ikpoba River, Ogba Stream and Osse stream. Many depositional land forms results especially flood pains characterized with point bar, islets, levees, back swamps and channel filling, alluvial fan and Delta.

The local relief in the City is 91 meters above sea level. A topographical map of the city on a scale of 1,277,778 produced by Balasha-Jalon consultants shows that the city contains 15 local depressions which may have been formed during the arching in the Neogene of the lower Tertiary Beds (Odemerho, 1988).

1.7.3 Soil Properties

Benin City is underlain by sedimentary rock of the Miocene-Pleistocene age often referred to as the Benin formations. This formation is dominantly arenaceous comprising of soft, poorly sorted, unconsolidated, cross bedded, occasionally pebbly yellow and white sands. The soils developed on Benin formation around the city belong to the Kulfo series (Moss, 1957). The soils are reddish

brown clayey sand, to depths of more than 10 m and have low silt content while clay fraction increases. However, with severe compaction under urban land use, the top soils acquire higher values of bulk density, and thus become relatively impermeable so that whenever its rains, runoffs are generated which subsequently produced gullies in the area.

1.7.4 Vegetation Cover

The relationship between vegetation and soil erosion, between cultivation and soil loss are well known (Osterkamp and Toy, 1997). It has been realized that forest soils become more erodible when put under cultivation. Changes in vegetation cover bring about direct and indirect changes in the soil environment which leads to an alteration in the structural organization of the soil. The tropical rainforest vegetation is noticeable in the area of study. The predominant vegetation here is the moist deciduous forest which is rich in timber resource.

1.8 GEOLOGY OF THE STUDY AREA

The Geology of the study area is characterised by the geology of Niger Delta. The Niger Delta is situated in southern Nigeria between latitudes 3°N and 6°N and longitude 5° E and 8° E (Nwachukwu, and Chukwura, 1986). It covers an area of 75,000sqkm. It is bounded to the west and northwest by the western African shield, which terminates at the Benin hinge line and to the east, by the Calabar hinge line. The Anambra basin and Abakaliki anticlinorium mark its northern limit. To the south, it is bounded by the gulf of Guinea. The Niger Delta Basin to date is the most prolific and economic sedimentary basin in Nigeria by virtue of the size of petroleum accumulations, discovered and produced as well as the spatial distribution of the petroleum resources to the Onshore, Continental shelf through deepwater terrains. Intensive exploration efforts over the last 35 years in and around the Niger Delta in particular has led to a succession of significant discoveries, notably the Bonga, Agbami/Ekoli and Akpo discoveries in Nigeria and

Zafiro and Alba in Equatorial Guinea. However, the full potential of the continental slope and rise seaward of the shelf break is only recently becoming apparent, with a number of exploration programs having resulted in world-class discoveries being made in recent years. From the Eocene to the present, the delta has prograded southwestward, forming depobelts that represent the most active portion of the delta at each stage of its development (Doust and Omatsola, 1990).These depobelts form one of the largest regressive deltas in the world with an area of some 300,000 Km2 (Kulke, 1995 and Chukwueke, 1997), a sediment volume of 500,000Km, and a sediment thickness of about 12km in the basin depocenter. Three major sedimentation cycles have been established in the Niger delta as well as other parts of the southern Nigerian sedimentary basin. These are:

(i) Lower Cretaceous to Santonian cycle, (ii) Campanian to Paleocene cycle and (iii) Paleocene/Lower Early Eocene to Recent (Youngest)

The third sedimentary cycle, which started in the Paleocene/Early Eocene, is responsible for the main part of the delta's growth (Short & Stauble, 1967).

The Niger delta oil province with its commercial oil fields is confined to the area covered by a thick sequence of rocks belonging to the youngest (Tertiary) sedimentary cycle. Megatectonically, the Niger delta is framed by a set of older and stable megatectonic elements that enhanced and controlled the development of the present day Niger delta (Fig. 2). Rift faulting during the Precambrian developed these structures (Weber, 1971). Deep-seated faults associated with this rifting controlled the outlines of the delta.

These structures are

(i) the Benin flank, a NE – SW trending flexure or fault zone called the Benin Hinge Line,

(ii) the Calabar flank N.W-SE hinge line which is the subsurface continuation of the Oban Massif. It marks the eastern fringe of the delta,

(iii) the Senonian Abakaliki uplift and (iv) the post Abakaliki Anambra Basin.

These units are found to the north of the delta, and were also stable elements throughout the Cenozoic

1.8.1 Stratigraphy

Since the inception of the Cenozoic delta in the Paleocene/Lower Eocene, the history has been one of a major regression with a gradual southward offlap of thin, quite extensive lenses of sediments formed as result of deposition occurring simultaneously under full terrestrial (fluviatile) conditions with the interplay between terrestial and marine influence (i.e. paralic) and under fully marine conditions (Frankl & Cordry 1967). Thus the sequence observed laterally (i.e. starting with coarse sandy deposits and ending with marine clays) is also observed vertically in the Niger delta. In a cross-section, a time stratigraphic unit of such deltaic sediment is characteristically S-shaped or sigmoidal (Merki, 1972). The formations are therefore strongly diachronous, their ages becoming progressively younger in a downdip direction and ranging from Paleocene to Recent. Thus the established tertiary sequence in the Niger delta demonstrates a tripartite lithostratigraphic succession from marine prodeltaic shale (Akata Formation) through a sand/shale paralic unit (Agbada Formation) to continental sands (Benin Formation). The strata compose and estimated 8535 m of the section at the approximate depocentre in the central part of the delta (Short and Stauble, 1967). The characteristic features of these formations are outlined below:

1.8.2 Akata Formation

It is characterized by a uniform shale development. The formation is a marine sedimentary sequence laid down in front of an advancing delta. These prodeltaic shales are medium to dark grey, fairly hard or at places soft, gumbo-like and sandy or silty in several places, the shales of this formation were found to be undercompacted, and therefore mobile, and may contain lenses of

abnormally high-pressured siltstone or fine-grained sandstone (Allen, 1965; Reyment, 1965; Short & Stauble, 1967 and Oomkens 1974).

The upper boundary of the formation has been structurally deformed, while diaprism and high-pressure zones developed in it, on a large scale. Generally, the Akata Formation contains rich foraminiferal fauna. Planktic foraminifera may constitute more than 50 % of the microfauna. The benthonic foraminiferal assemblages indicate that the shale was deposited on a shallow marine shelf and slope. The Akata Formation is considered to be the main source rock in the Niger delta (Evamy *et al.*, 1978; Bustin 1988 and Schlumberger, 1985). The known age of the Akata Formation is Eocene to Recent (Asseez, 1976; Doust and Omatsola 1990).

The shale is continuous in the subsurface with its probable outcrop equivalent the Paleocene/Eocene Imo Formation. The complex movements of the Niger delta sediments are controlled by the adjustments of the shale either by the downward movements in response to the pressure impacted by the overlying sediments or lateral motion of the shale on the continental slope or its upward diapiric motion. These movements are believed to have assisted in the formation of the growth faults and roll over structures, which are common features of the main Niger delta basin.

1.8.3 Agbada Formation

This sequence of strata forms the hydrocarbon prospective sequence in the Niger delta. The formation is characterized by alternating sandstones and shales of the delta front, distributary channel, and deltaic plain origin. Weber (1971) showed that the alternating sequence of sandstones and shales of the Agbada Formation is of cyclic sequences of marine and fluvial deposits. The sand content ranges from 50 to 75 %. The sandstones are medium to fine grained, fairly clean locally calcareous, and shelly. They consist dominantly of quartz and potash feldspar with

subordinate and illite. The shales are dark to grey, fairly consolidated and silty with local glauconite. They consist dominantly of kaolinite (average value 73 %) with small amount of mixed layers of illite and montmorillonite. The formation has a maximum thickness of 3940 meters at the central part and thins northwards and towards the North western and Eastern flanks of the delta. Although, the thickest known section is about 3480 meters, the maximum thickness may well be much greater (Short and Stauble 1967). Generally, the boundary between the sand and shales is sharp. Where the sands grade into shales, shell fragments, glauconites, limonite coatings are common. The shales are denser at the base than higher up in the column because of compaction. They become silty and sandy towards the Benin Formation while shaliness increases downwards and laterally into the Akata Formation.

The Agbada shales contain microfauna that are best developed at the base of individual shale units. The depth of the fossil assemblage ranges from littoral estuarine to marsh types of fauna developed at a water depth of approximately 100 meters. The slightly consolidated sand has a calcareous matrix, but most of the sand is unconsolidated. The coarse and poorly sorted sand indicates a fluviatile origin while the well-sorted sand represents beach or coastal barrier deposits. The mature Eocene to Miocene shales interbedded within the deltaic sands in the lower part of the paralic sequence is considered to be a major source rock. (Nwachukwu & Chukwura, 1986; Knox & Omatsola 1989; Shannon & Naylor 1989: Doust & Omatsola 1990 and Reijers 1996). The Agbada Formation is held to contain most of the reservoir rocks of the Niger delta. The porosity is of excellent quality (ranging between 28 and 32 %) while permeability is in the darcies. Reservoir quality is closely dependent on the depositional environment. The Agbada Formation is less carbonaceous and more marine than overlying Benin Formation there is also an increase ion microfauna with depth. This could be an indication of increasing rate of sedimentation and changes

in salinity and temperature of the delta front. The age of the Agbada Formation varies from Eocene to Recent.

1.8.4 Benin Formation

This is the uppermost unit of the Niger delta complex. The formation can be easily distinguished based on its high sand percentage (70 – 1000 %). The sand is dominantly massive highly porous and freshwater bearing with locally interbedded shale beds, which are considered to be of braided stream origin. The sands are poorly sorted, ranging from fine to coarse – grained and occasionally pebbly and they contain abundant wood, fragments, which become lignitic with depth. Composition, structure and grain size show deposition in a probably upper deltaic environment. The thickness is variable and may be more than (1990 m) in Warri – Degema area. Most companies exploring for oil in the Niger delta, arbitrarily define the base of the Benin Formation by the deepest fresh - water – bearing sandstone that exhibits high resistivity. Short & Stauble (1967), however, defined the base of the Benin Formation by the first marine foraminifera within shale, as the formation is non-marine in origin. Avbovbo (1978) partly agrees with Short & Stauble (op cit) but also demonstrated that the base of the fresh water in the delta sediments extends into the Agbada Formation and thus not coincident with the base of the Benin Formation. The Benin Formation is deposited across the entire Niger delta. It is a continental deposit and consists of various structures such as natural levees channel fills, ox-bow fills etc. these structures indicate a variability of the shallow water depositional medium (Short & Stauble, 1967). It becomes progressively younger from North towards the South.

1.9 AIM AND OBJECTIVES

The aim focuses on assessing the subsurface stratigraphy using 2D electrical resistivity imaging (ERI) techniques.

The objectives of this research are to;

1. conduct electrical resistivity imaging (ERI) surveys in selected locations in Benin City to generate data on subsurface resistivity profiles.
2. analyze and interpret the resistivity data obtained from the ERI surveys, identifying distinct subsurface layers and their variations in resistivity.
3. correlate the resistivity data with known geological formations in the study area, and interpret the layers in terms of their composition (e.g., soil, rock, groundwater, etc.).
4. map the subsurface stratigraphy of the study area, identifying the depth, thickness, and extent of different geological units.

CHAPTER TWO

LITERATURE REVIEW

2.1 PREVIOUS WORK DONE

Aigbogun and Egbai carried out a geophysical survey in 2012. Investigating the underlying geology properties of the aquifer layers was the aim of the geophysical survey. An ABEM 1000C Terrameter with an integrated booster was used for the investigation. Eighty carefully selected locations were subjected to Vertical Electrical Sounding (VES) using the Schlumberger array. The geolocation data for the VES stations was obtained using the GPS map 76csx. The maximum current electrode spacing was 1,362 metres, with three exceptions (VES 13, 510 metres, VES 14, 430 metres, and VES 17, 928 metres). The examination yielded the following conclusions: the studied region is constituted of 5-8 earth strata with a range of resistivities (115 Ωm-18,111.8 Ωm), thicknesses (13.7 m-181.6 m), and depths (38.9 m-198.6 m). AAK, AAAK, AKQH, KQQH, AAKH, AKQ, AKQQ, AAKQ, HAKQH, AAKQH, and HKHAKQ were the types of curves that were present. The ascending A-type is present in the majority of the curves, indicating a homogeneous earth that is stratified horizontally.

A 2013 study by Arjwech et al. evaluated the use of 2D and 3D electrical resistivity imaging (ERI) to accurately determine the depth of unidentified bridge foundations. In the context of challenging terrain, a survey approach for mixed terrain/water situations is outlined. While some electrodes are designed to be used underwater, others are placed on the banks of the stream. Tests were carried out at five field locations, which included a railway bridge, three road bridges, a geotechnical test site, and spread footings with both known and unknown depths. The dipole-dipole setup was used to acquire the 2D data. The bigger bridge foundations' shape and depth extent were accurately resolved using the 2D ERI approach, but the smaller foundations' shape and depth extent were less

precisely resolved. The 3D ERI technique takes a lot of time and doesn't provide enough advantages over 2D ERI to be useful for investigating unknown bridge foundations. Bridge engineers can employ the comparatively simple and cost-effective 2D ERI geophysical approach with ease.

In 2012, Gómez-Ortiz and Martín-Crespo conducted a study. There are many carbonate rock outcrops in Segovia Province, Spain, that are impacted by karstification processes. These outcrops include a large number of galleries, caves, and sinkholes. In the instance of the Sima de Madrona sinkhole collapse, dolostone sinking is to blame. The purpose of this study was to use shallow, non-invasive geophysical techniques, such as ground penetrating radar and electrical resistivity tomography, to determine the presence and features of cavities and galleries as well as to assess the danger of subsidence in the area. The optimal combination of inquiry depth (up to 8 metres) and resolution required to photograph tiny to medium-sized cavities (~1 to 4 metres) has been achieved with the combined application of these two separate shallow geophysical techniques. The cavities identified here influence a variety of anthropogenic objects, including a roadway and agricultural areas, making the associated concerns obvious.

Alile and Abraham (2015) created photographs of the subsurface structure of the University of Benin's capitol gate area in Edo State, Nigeria, using 2D and 3D resistivity imaging techniques. Geophysical exploration uses straightforward, quick, low-cost, and reasonably accurate resistivity imaging methods in both 2D and 3D. Two-dimensional geoelectrical resistivity field data were gathered in an orthogonal set using the traditional Wenner array setup. Using a 3D inversion code, the observed 2D apparent resistivity values were converted into a 3D data set. The inverted 3D model resistivity images are displayed as block images and as horizontal and vertical depth slices.

The usefulness of employing parallel 2D profiles for 3D geoelectrical resistivity imaging has been demonstrated in this study.

At the proposed location of the KNUST Teaching Hospital Building in Kumasi, Ghana, Andrews et al. (2013) conducted a geophysical investigation using 2D and 3D electrical resistivity imaging techniques to study the nature of the subsurface structure and assess its suitability for the construction of superstructures. There was an old garbage dump on the property. The principal aims are to ascertain the depth to bedrock and the potential existence of faults, fractures, voids, and clay that could endanger the proposed constructions. Using the Wenner setup, twenty-eight (28) high-resolution 2D electrical resistivity pictures were obtained, with electrode and profile separations of 4 m. The 200 m constant profile length for each line was covered using the roll-along technique. A 3D picture was created by combining and inverting the 2D resistivity data. The locations of bedrock, cracks, clay soil, and seepage routes from the former waste dump were made possible by the 2D and 3D models. The site is appropriate for the planned KNUST Teaching Hospital, according to the findings.

2.2 BASIC PRINCIPLES OF ELECTRICAL RESISTIVITY

Electrical properties of earth materials Electric current flows in earth materials at shallow depths through two main methods. They are electronic conduction and electrolytic conduction. In electronic conduction, the current flow is via free electrons, such as in metals. In electrolytic conduction, the current flow is via the movement of ions in groundwater. In environmental and engineering surveys, electrolytic conduction is probably the more common mechanism. Electronic conduction is important when conductive minerals are present, such metal sulfides and graphite in mineral surveys. The resistivity of common rocks, soil materials and chemicals (Keller and Frischknecht 1966, Daniels and Alberty 1966, Telford et al. 1990). Igneous and metamorphic rocks

typically have high resistivity values. The resistivity of these rocks is greatly dependent on the degree of fracturing, and the percentage of the fractures filled with ground water.

Table 2.1: Resistivities of common geologic materials (Source: An Introduction to Applied Environmental Geophysics, John M. Reynold, 1997

Material	**Nominal resistivity (Ωm)**
Quartz	$3 \times 10^2 - 10^6$
Rock salt	$3 \times 10 - 10^{13}$
Anthracite	$10^{-3} - 2 \times 10^5$
Lignite	$9 - 2 \times 10^2$
Granite	$3 \times 10^2 - \times 10^6$
Granite (weathered)	$3 \times 10 - 5 \times 10^2$
Sycnite	$10^2 - 10^6$
Diorite	$10^4 - 10^5$
Gabbro	$10^3 - 10^6$
Basalt	$10 - 1.3 \times 10^7$
Schists (calcareous and mica)	$20 - 10^4$
Schist (graphite)	$10 - 10^2$
Slates	$6 \times 10^2 - 4 \times 10^7$
Marble	$10^2 - 2.5 \times 10^8$
Consolidated shales	$20\,2 \times 10^3$
Conglomerates	$2 \times 10^3 - 10^4$
Sandstones	$1 - 7.4 \times 10^8$
Limestones	$5 \times 10 - 10^7$
Dolomite	$3.5 \times 10^2 - 5 \times 10^3$
Marls	3.7×10
Alluvium and sand	$10 - 8 \times 10^2$
Moraine	$10 - 5 \times 10^3$
Sherwood sandstone	100 – 400

Soil (40% clay)	8
Soil (20% clay)	33
Top soil	250 – 1700
London clay	4 – 20
Lias clay	10 – 15
Boulder clay	15 – 35
Clay (very dry)	50 – 150
Mercia mudstone	20 – 60
Coal measures clay	50
Middle coal measures	>100
Chalk	50 – 150
Coke	0.2 – 8
Gravel (dry)	1400
Gravel (saturated)	100
Quaternary/recent sands	50 – 100
Laterite	800 – 1500
Laterite soil	120 – 750
Dry sandy soil	80 – 1050
Sand clay/clayey sand	30 – 450
Sand and gravel	30 – 225
Unsaturated landfill	30 – 100
Saturated landfill	15 – 30
Acid peat water	100
Acid mine waters	20
Rainfall runoff	20 – 100
Landfill runoff	<10 – 50

2.3 CURRENT FLOW IN A HOMOGENEOUS ISOTROPIC MEDIUM

When two current electrodes are moved in close proximity to one another, current flows along arc-shaped paths connecting the two electrodes. If the earth has a constant resistivity, about 50% of the current flows through rock at depths shallower than the current electrode spacing. In fact, in order for at least 50% of the current to flow through an interface at a depth of z meters into a second medium, the current electrode separation needs to be at least twice and preferably more than three times-the depth. What this implies is that by increasing the electrode spacing, more of the injected current will flow to greater depths. This has obvious practical implications, particularly when dealing with situations where the depths are of the order of several hundreds of meters, so requiring very long cable lengths that can produce undesirable inductive coupling effects. Because the total resistance in the electrical path increases as electrode spacing is increased, to get current to flow over these longer paths requires a larger generator of electrical current. Thus, the maximum distance that current electrodes can be separated by is in part dictated by the size of the generator used to produce the current.

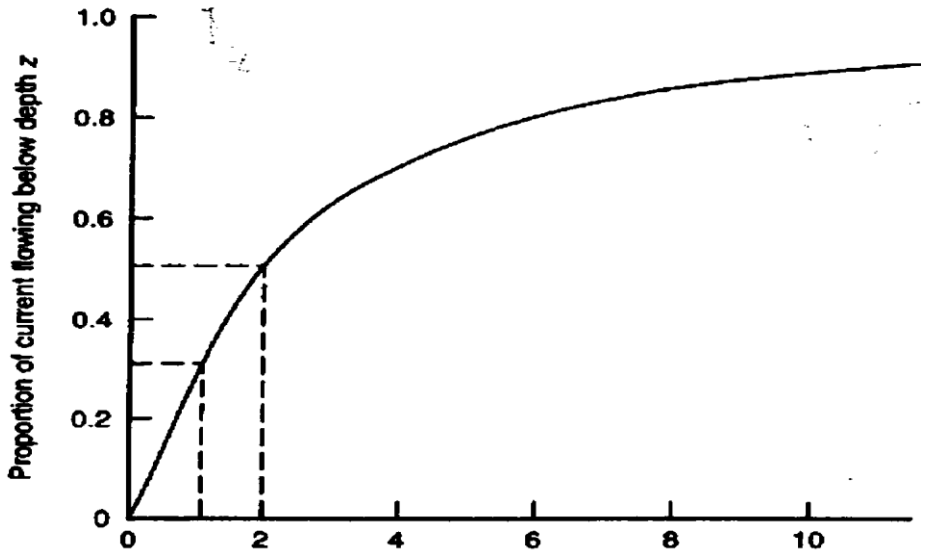

Figure 2.1: Proportion of current flowing below a depth z (m); $\frac{AB}{2}$(m) is the current electrode separation (Source: An Introduction to Applied and Environmental Geophysics by J.M Reynolds, 1996)

Assuming for a moment that we have a large enough generator to produce a measurable current in the ground at large current electrode spacing, this increase in the depth of current penetration as current electrode spacing increases suggests a way in which we could hope to decipher the resistivity structure of an area. Because current flows mostly near the Earth's surface for close electrode spicing, measurements of apparent resistivity at these electrode spacings will be dominated by the resistivity structure of the near surface. If the current and potential electrodes are spread apart and the apparent resistivity remeasured, these measurements will incorporate information on deeper Earth structure.

For very deep soundings where the electrode separation is more than several kilometers, telemetering the data becomes the only practical solution (Shabtaie *et al.*,1982). However, it should

be emphasized that it is misleading to equate the depth of penetration with the current electrode separation as a general rule of thumb in the region of a resistivity survey

2.3.1 Current Flow in Layered Media

In the previous section, we assumed that the Earth has a constant resistivity. Obviously, this is not true or else we would not be trying to map the variation in resistivity throughout the Earth. To understand the reason for this discrepancy in apparent resistivities, we must know the difference between geologic sections and geoelectric sections.

A geoelectric section describes the electrical boundaries (resistivities) of rocks in a vertical section through the crust, while a geologic section describes boundaries based on age and/or lithology which do not necessarily coincide with boundaries identified electrically. Furthermore, different lithologies can have the same resistivity and thus would form only one electric unit. A geoelectric unit is characterized by two basic parameters: the layer resistivity (ρ_i and the layer thickness (t_i) for the *i*th layer ($i = 1$ for the surface layer). A section of a geoelectric unit is shown in the figure below.

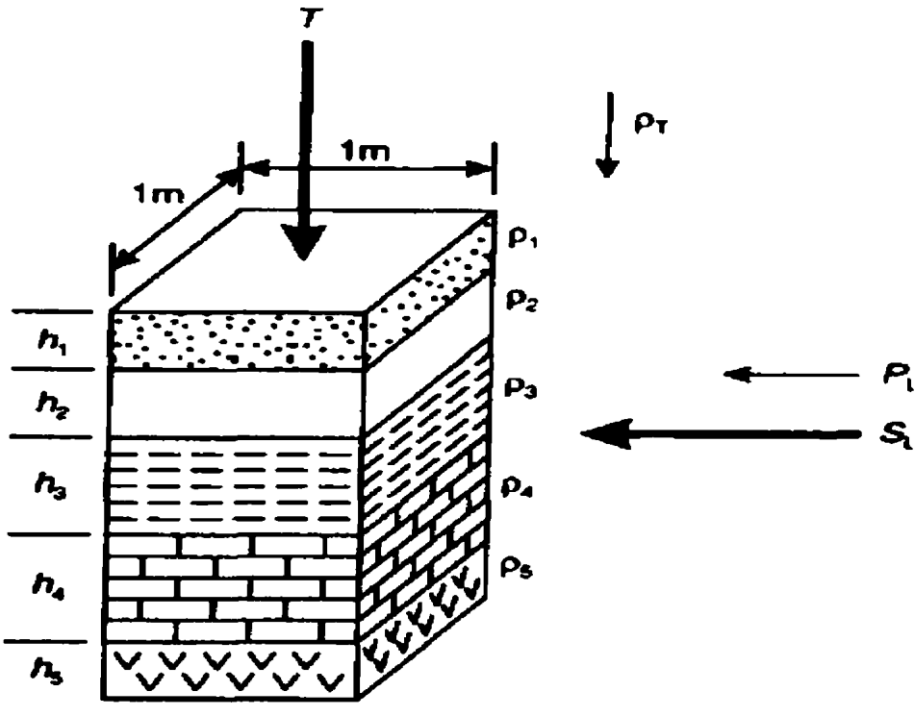

Figure 2.2: A geoelectric section showing thickness (h) and true resistivity (**ρ**) of component layers with an indication of the total longitudinal conductance (S_L) and total transverse resistance (T); subscripts L and T refer to longitudinal and transverse, respectively.

For a layered sequence, there are five parameters depending on whether the current is flowing normal (transverse) or parallel (longitudinal) to the bedding; these are called the longitudinal conductance (S_L; units mS); transverse resistance (T; units Ωm^2); longitudinal resistivity (ρ_L; units Ωm); transverse resistivity (ρ_T; units Ωm); and anisotropy. We consider vertical section of unit area normal to the bedding as shown in **Figure 2.2** above.

The resistance of a single layer, i is by definition given by;

$$R_i = \left(\frac{\rho_i l}{A}\right) = \rho_i h_i \qquad (2.1)$$

Since for a unit area, $A = 1m^2$ and $l = h_i$ for ith layer.

For current flowing in the transverse direction, the resistances are in series and transverse resistance T is given by

$$T = \sum_{i=1}^{m} \rho_i h_i \tag{2.2}$$

For each layer, $R = \rho h$ and $\rho = R/h$. For the whole section, we may define an average transverse resistivity by the equation (2.13) below.

$$\rho_T = \frac{\sum_{i=1}^{m} \rho_i h_i}{\sum_{i=1}^{m} h_i} = \frac{T}{H} \tag{2.3}$$

Where $H = \sum_{i=1}^{m} h_i$

For current flowing along the bedding planes, the resistances are effectively in parallel. Thus,

$$\frac{1}{R} = S_L = \sum_{i=1}^{m} \frac{1}{R_i} = \sum_{i=1}^{m} \frac{h_i}{\rho_i}$$

$$S_L = \sum_{i=1}^{m} \frac{h_i}{\rho_i} \tag{2.4}$$

Where S_L is longitudinal conductance

From equation (2.4), we define average longitudinal conductivity (i.e. conductance per unit thickness) as

$$\sigma_L = \frac{S}{H} \tag{2.5a}$$

〖Hence, longitudinal resistivity is given by

$$\rho_r = \frac{1}{\sigma_L} = \frac{H}{S} = \frac{\sum h_i}{\sum \frac{h_i}{\rho_i}} \tag{2.5b}$$

The dependence of resistivity on direction of current flow is called anisotropy. We define the coefficient of anisotropy as (λ), which is given by the expression

$$\lambda = \sqrt{\frac{\rho_T}{\rho_L}} = \sqrt{\frac{ST}{H^2}} \tag{2.6}$$

If $\lambda > 1$, the region is anisotropic

$\lambda = 1$, the region is isotropic.

T, ρ_T, S_L , ρ_L and λ are geoelectric parameters.

The sums of all the longitudinal conductance and of the transverse resistances for a layered ground are called the Dar Zarrouk 'function' and 'variable', respectively. The importance of the longitudinal conductance for a particular layer is that it demonstrates that it is not possible to know either the true layer conductivity (or resistivity) and the layer thickness, so giving rise to layer equivalence. For example, a layer with a longitudinal conductance of 0.05mS can have a resistivity of l00Ωm and thickness 5m. Layers with the combination of resistivity 80Ωm and thickness 4m, and 120Ωm and 6m, are all equivalent electrically. Equivalence needs to be considered during interpretation of sounding curves and generally in the interpretation of electrical data, whether obtained by contact electrical or electromagnetic induction methods.

Where a point current source is located close to a plane boundary between two homogeneous media, the lines of current flow (and hence of equipotential) are refracted at the boundary in proportion to the contrast in resistivity between the two media. Shown below are current-flow paths from two current electrodes in two simple two-layer models.

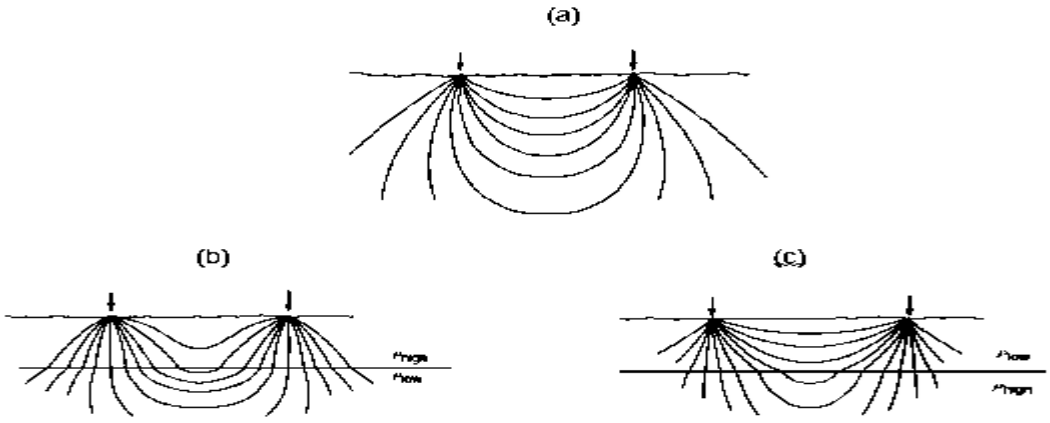

Figure 2.3: Current flow patterns for (a) uniform half-space; (b) two-layer ground with higher resistivity in upper layer; (c) two-layer ground with lower resistivity in upper layer.

The model (b) contains a high-resistivity layer overlying a lower resistivity layer. This model is characteristic of the resistivity profile that would be found in a region where unsaturated alluvium overlies water saturated alluvium. The model (c) contains a low resistivity layer overlying a higher resistivity layer. This model is characteristic of a perched aquifer. For comparison, a model, (a) representing the paths that current would have flowed along if the Earth had a constant resistivity equal to that of the top layer.

It will be observed that the current flow in the layered media deviates from that observed in the homogeneous media. In the layered media, the current flow lines are distorted in such a way that current preferentially seems to be attracted to the lower-resistivity portion of the layered media. In the model (b), current appears to be pulled downward into the lower resistivity layer. In the model (c), current appears to be bent upward, trying to remain within the lower resistivity layer at the top of the model. This is due to the current's preference toward flowing through the path of least

resistance. For the model (b), that path is through the deep layer. For the model (c), that path is through the shallow layer.

2.3.2 Variation in Apparent Resistivity and Measured Potential for Layered Media

An important consequence of the deviation in current flow in layered media is how it can affect our measurements of apparent resistivity. If we configured an electrical experiment over these two models by measuring the potential difference at two places on the surface of the earth between the two current electrodes and then computed the apparent resistivity, because current is preferentially being pulled into the lower layer for the model (b), the current density between the two current electrodes near the surface of the Earth (where we are measuring electrical potential) will be smaller than that which would be observed if the Earth were homogeneous. By the same token, for the model (c), the current density would be higher than that observed in a homogeneous Earth, because the current is being preferentially channeled through the near-surface layer.

Thus, for model (b), the potential difference will be smaller than would have been observed in a homogeneous Earth, because the current density is smaller than that which would have been observed in a homogeneous Earth. Therefore, the measured apparent resistivity will be decreased. Conversely, for model (c), the potential difference will be larger than that observed in a homogeneous Earth, and the measured apparent resistivity will likewise be larger.

The potential at a point adjacent to the plane boundary between two or more layers can be calculated using optical image theory. The interface AB is regarded as a semi-transparent mirror with reflection coefficient k and transmission coefficient $1-k$. If a current source of strength S is placed in one medium of resistivity ρ_1, the source's image point lies in the second medium of resistivity ρ_2 (where $\rho_2 > \rho_1$) but has a reduced strength kS, where k is dependent upon the resistivity contrast between the two media and lies in the range ± 1. This k factor is akin to the

reflection coefficient in optics and in reflection seismology. Above the interface, the effect of the boundary is by reflection while below is by transmission.

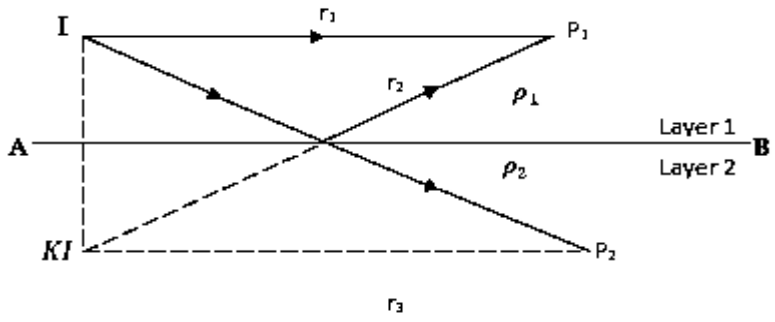

Figure 2.4: Method of optical images for the calculation of a potential at a point

In the first medium.

$$V_{P_1} = \frac{\rho_1 I}{2\pi}\left(\frac{1}{r_1} + \frac{k}{r_2}\right) \tag{2.7}$$

In the second medium,

$$V_{P_2} = \frac{\rho_2 I}{2\pi}\left(\frac{1-k}{r_3}\right) \tag{2.8}$$

To find *k*, we must use the boundary conditions at the interface i.e. the potential is continuous across the boundary so that if $P_1 = P_2$, with both at the boundary, then

$$V_{P_1} = V_{P_2} \text{ and } r_1 = r_2 = r_3 = r$$

$$\frac{\rho_1 I}{2\pi}\left(\frac{1}{r} + \frac{k}{r}\right) = \frac{\rho_2 I}{2\pi}\left(\frac{1-k}{r}\right)$$

$$\frac{\rho_1 I}{2\pi r}(1+k) = \frac{\rho_2 I}{2\pi r}(1-k)$$

Multiplying both sides by $2\pi r/I$ gives

$$\rho_1(1+k) = \rho_2(1-k)$$

$$\frac{\rho_2}{\rho_1} = \frac{1+k}{1-k} \tag{2.9}$$

By cross multiplying,

$$\rho_1(1+k) = \rho_2(1-k)$$

$$\rho_1 + k\rho_1 = \rho_2 - k\rho_2$$

$$\rho_2 - \rho_1 = k\rho_1 + k\rho_2 = k(\rho_1 + \rho_2)$$

$$k = \frac{\rho_2 - \rho_1}{\rho_1 + \rho_2}$$

If the current passes from a lower resistivity medium to one with a higher resistivity, *k* is positive; if it passes into a medium with a lower resistivity, *k* is negative.

If $\rho_2 \to \infty$, then *k* = 1, i.e. dividing equation (2.41) by ρ_2 gives

$$k = \frac{\rho_2/\rho_2 - \rho_1/\rho_2}{\rho_2/\rho_2 + \rho_1/\rho_2} = \frac{1 - \rho_1/\rho_2}{1 + \rho_1/\rho_2}$$

as ρ → ∞,

$$k = \frac{1 - \rho_1/\infty}{1 + \rho_1/\infty} = \frac{1}{1} = 1$$

To calculate V_p, we usually sum the contribution of an infinite number of virtual sources produced by successive reflections at ρ_a/ρ_1 and ρ_1/ρ_2 interfaces. For reflection at ρ_a/ρ_1 for a source below, $k = 1$ as $\rho_1 \to \rho_2 \to \infty$.

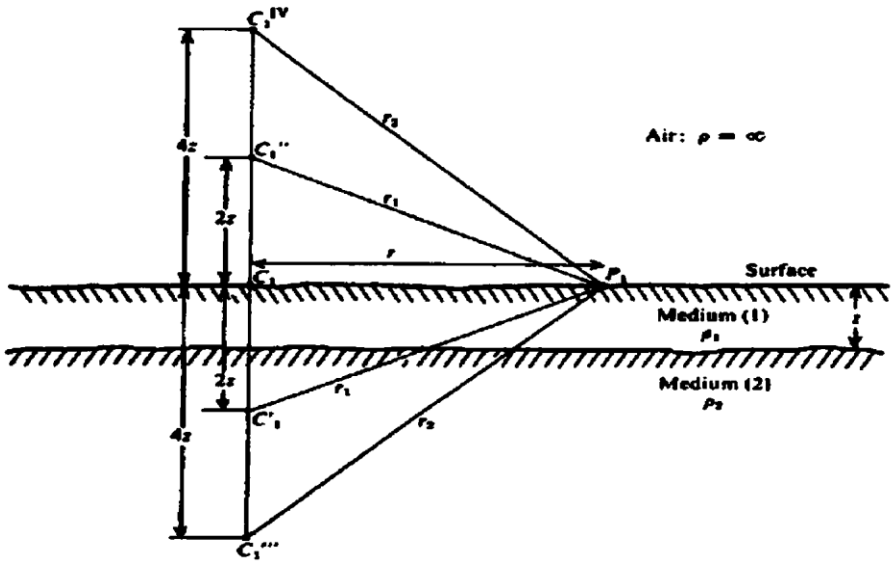

Figure 2.5: Images resulting from two horizontal beds.

Source $C_1$is produced by current I, at distance r from point P_1.

Source C_1^I is produced by reflection at ρ_1/ρ_2 boundary by current kI.

Source C_1^{II} is produced by reflection at ρ_2/ρ_1 boundary by current kI.

Source C_1^{III} is produced by reflection at ρ_1/ρ_2 boundary by current k^2I.

Source C_1^{IV} is produced by reflection at ρ_2/ρ_1 boundary by current k^2I.

So we have one source at distance r, produced by current I. Using Pythagoras theorem, we have, two sources at distance $[r^2 + (2z)^2]^{1/2}$ each from P_1, are produced by current kI, and then two sources at distance $[r^2 + (4z)^2]^{1/2}$ each from P_1, are produced by current k^2I. Generally, we have two sources at distance$[r^2 + (2nz)^2]^{1/2}$, produced by current k^nI, and the potential at P_1 is given by

$$V_P = \frac{\rho_1 I}{2\pi}\left(\frac{1}{r} + \frac{2k}{[r^2 + (2z)^2]^{1/2}} + \cdots + \frac{2k^n}{[r^2 + (2nz)^2]^{1/2}}\right)$$

Using the summation sign, this series can be written in the compact form

$$V_P = \frac{\rho_1 I}{2\pi r}\left(1 + 2\sum_{n=1}^{\infty} \frac{k^n}{\left[1+\left(\frac{2nz}{r}\right)^2\right]^{1/2}}\right) \quad (2.10)$$

This series is convergent, because $|k| < 1$, whereas the denominator increases indefinitely. The number of terms necessary to get a reasonable answer depends mainly on the value of *k* and partly on the ratio *z/r*. For a fixed value of *r*, the potential differs from that measured over uniform ground. For a uniform (homogenous, isotropic) earth, the potential is given by the first term in the above Equation ($\rho_1 I/2\pi r$) which is called the normal potential. The portion expressed by the infinite series is the disturbing potential which is the contribution of the reflection effect of the two interfaces. When *k* is positive and approximately unity, the total potential at *P* may be increased by a factor of 2 or more.

2.6 EXPRESSION FOR THE GEOMETRIC FACTOR (K)

Geometric factor (K_g) is a numerical multiplier defined by the geometrical spacing between electrodes, which is used in conjunction with the voltage-to-current (*R*) ratio measured in electrical resistivity surveys to give an apparent resistivity (ρ_a) such that

$$\rho_a = K_g \times R. \quad (1.11)$$

Recall that

$$\Delta V_{MN} = \frac{\rho I}{2\pi r}\left[\left(\frac{1}{AM} - \frac{1}{NB}\right) - \left(\frac{1}{MB} - \frac{1}{AN}\right)\right]^{-1}$$

Mathematically;

$$\Delta V = I\rho K \quad (1.12)$$

K is a geometric factor (including the factor $1/2\pi$), which depends upon the locations of electrodes and its given by;

$$K = 2\pi\left\{\left[\frac{1}{AM} - \frac{1}{MB}\right] - \left[\frac{1}{AN} - \frac{1}{NB}\right]\right\}^{-1} \quad (2.13)$$

2.6.1 Obtaining the Expression for the Geometric Factor of some Electrode Array Configurations

1. Wenner Array

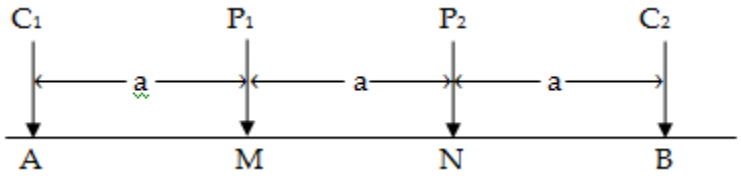

Figure 2.6: A Schematic of the electrode array configuration when using the Wenner array

Recalling Equation 2.13,

$$K = 2\pi\left\{\left[\frac{1}{AM} - \frac{1}{MB}\right] - \left[\frac{1}{AN} - \frac{1}{NB}\right]\right\}^{-1}$$

Where *AM*, *AN*, *BM*, and *BN* are the distances between the current electrodes, *A* and *B*, and the potential electrodes, *M* and *N* as shown in the figure above. From the diagram, $AM = NB = a$ and $AN = MB = 2a$. Therefore, Equation 2.11 becomes

$$K = 2\pi\left\{\left[\frac{1}{a} - \frac{1}{2a}\right] - \left[\frac{1}{2a} - \frac{1}{a}\right]\right\}^{-1} = 2\pi\left[\frac{1}{a} + \frac{1}{a} - \frac{1}{2a} - \frac{1}{2a}\right]^{-1}$$

$$= 2\pi\left[\frac{2}{a} - \frac{1}{a}\right]^{-1} = 2\pi\left[\frac{2-1}{a}\right]^{-1} = 2\pi a$$

Therefore the geometric factor for the Wenner array configuration is given by the expression $K = 2\pi a$. It is easy to show that when an "n" factor is included, to increase the electrode spacing for deeper current penetration, the K factor becomes $K = 2\pi an$.

2. Wenner-Schlumberger Array

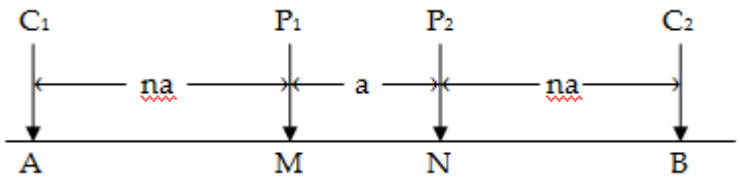

Figure 2.7: A Schematic of the Wenner-Schlumberger array electrode configuration

Recalling Equation 2.13,

$$K = 2\pi\left\{\left[\frac{1}{AM} - \frac{1}{MB}\right] - \left[\frac{1}{AN} - \frac{1}{NB}\right]\right\}^{-1}$$

Where *AM*, *AN*, *BM*, and *BN* are the distances between the current electrodes, *A* and *B*, and the potential electrodes, *M* and *N* as shown in the figure above. From the diagram, $AM = NB = an$ and $AN = MB = an + a = a(n+1)$. Therefore, Equation 2.11 becomes

$$K = 2\pi\left\{\left[\frac{1}{an} - \frac{1}{a(n+1)}\right] - \left[\frac{1}{a(n+1)} - \frac{1}{an}\right]\right\}^{-1} = 2\pi\left[\frac{1}{an} + \frac{1}{an} - \frac{1}{a(n+1)} - \frac{1}{a(n+1)}\right]^{-1}$$

$$= 2\pi\left[\frac{2}{an} - \frac{2}{a(n+1)}\right]^{-1} = 2\pi\left[\frac{2(n+1) - 2n}{an(n+1)}\right]^{-1}$$

$$= 2\pi\left[\frac{2}{an(n+1)}\right]^{-1} = \pi an(n+1)$$

Therefore the geometric factor for the Wenner-Schlumberger array configuration is given by the expression $K = \pi an(n+1)$. It is worthy of note that the conventional Wenner array (Wenner Alpha) is actually a special case of the Wenner-Schlumberger array where the n factor is equal to 1. This array effectively becomes the Schlumberger array when the n factor is greater than 2. Thus the Wenner-Schlumberger array is actually a combination of the Wenner and Schlumberger array adapted for use for an arrangement with a line of electrodes with a constant spacing (as normally used in 2-D electrical imaging).

3. Dipole-dipole Array

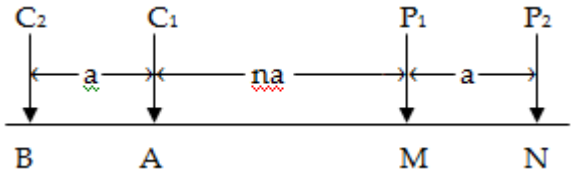

Figure 2.8: A Schematic of the electrode array configuration when using the Inline Dipole-dipole array

Recalling Equation 2.11,

$$K = 2\pi\left\{\left[\frac{1}{AM} - \frac{1}{MB}\right] - \left[\frac{1}{AN} - \frac{1}{NB}\right]\right\}^{-1}$$

where *AM, AN, BM,* and *BN* are the distances between the current electrodes, *A* and *B*, and the potential electrodes, *M* and *N* as shown in the figure above. From the diagram, $AM = na$ and $AN = MB = na + a = a(n+1)$ and $NB = na + 2a = a(n+2)$. Therefore, Equation 2.11 becomes

$$K = 2\pi\left\{\left[\frac{1}{an} - \frac{1}{a(n+1)}\right] - \left[\frac{1}{a(n+1)} - \frac{1}{a(n+2)}\right]\right\}^{-1}$$

$$= 2\pi\left[\frac{1}{an} - \frac{2}{a(n+1)} + \frac{1}{a(n+2)}\right]^{-1}$$

$$= 2\pi\left[\frac{(n+1)(n+2) - 2n(n+2) + n(n+1)}{an(n+1)(n+2)}\right]^{-1}$$

$$= 2\pi\left[\frac{n^2 + 3n + 2 - 2n^2 - 4n + n^2 + n}{an(n+1)(n+2)}\right]^{-1}$$

$$= 2\pi\left[\frac{2}{an(n+1)(n+2)}\right]^{-1} = \pi an(n+1)(n+2)$$

Therefore the geometric factor for the Inline Dipole-dipole array configuration is given by the expression $K = \pi an(n+1)(n+2)$.

4. Geometric Factor for Equatorial Dipole-dipole Array

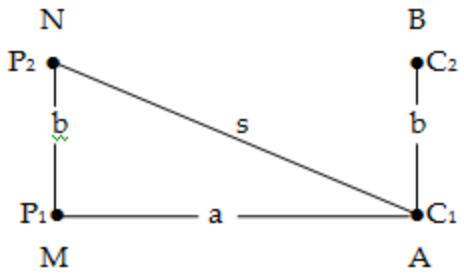

Figure 2.9: A Schematic of the electrode array configuration when using the Equatorial Dipole-dipole array

In this array, the electrode configuration is not symmetric. Hence Equation 2.13 becomes

$K = 4\pi\left\{\left[\frac{1}{AM} - \frac{1}{MB}\right] - \left[\frac{1}{AN} - \frac{1}{NB}\right]\right\}^{-1}$

where *AM, AN, BM,* and *BN* are the distances between the current electrodes, *A* and *B*, and the potential electrodes, *M* and *N* as shown in the figure above. From the diagram,

$AM = NB = a$ and $MB = AN = s$, where using Pythagoras theorem,

$$s^2 = a^2 + b^2 \quad \therefore s = \sqrt{a^2 + b^2}$$

$$K = 4\pi\left\{\left[\frac{1}{AM} - \frac{1}{MB}\right] - \left[\frac{1}{AN} - \frac{1}{NB}\right]\right\}^{-1} = 4\pi\left\{\left[\frac{1}{a} - \frac{1}{s}\right] - \left[\frac{1}{s} - \frac{1}{a}\right]\right\}^{-1}$$

$$= 4\pi\left[\frac{2}{a} - \frac{2}{s}\right]^{-1} = 4\pi\left[\frac{2s - 2a}{as}\right]^{-1}$$

$$= 4\pi\left[\frac{as}{2(s-a)}\right] = \frac{2\pi as}{s-a} \text{ where } s = \sqrt{a^2 - b^2}$$

Therefore the geometric factor for the Equatorial Dipole-dipole array electrode configuration is given by the expression

$$K = \frac{2\pi as}{s-a} \text{ where } \mathrm{s} = \sqrt{\mathrm{a}^2 - \mathrm{b}^2}$$

CHAPTER THREE

MATERIALS AND METHOD

3.1 EQUIPMENT USED

The equipment used for the electrical resistivity data collection was PASI Earth resistivity meter Basic field Equipment for this work include

- PASI Earth resistivity meter
- Booster
- Metal electrodes
- Cables
- Hammer
- GPS

(a) Pasi Earth Resistivity Meter

This terrameter provides a combined low/high power resistivity units that is fully self-contained and portable. It is a portable micro-processor controlled integrated receiver and transmitter which provide a digital read out of the current and potential difference. It has low operating frequency, which makes it to measure deeper. The instrument has Signal Averaging System (SAS) which ensures that consecutive readings are automatically taken out and the result averaged. Power is supplied by rechargeable battery pack. Several self-diagnostic checks are built in and error codes displayed for instrument, cable and electrode faults. The instrument supports the co-linear (Wenner, Schlumberger, Pole-Pole, Dipole-Dipole, Pole Dipole and Gradient) and the Non Linear (square) arrays

(b) Metal Electrodes:

These are usually made of stainless steel with tensil strength. They are hammered into the ground to about one third of its 0.8m length so as to make contact with the ground for effective current flow in the array used, two electrodes are for current and two others for potential flow

(c) Cables:

These are in reels, four reels are used. Large reels are for connection of the two current electrodes to the current terminals of the terrameter while the other two small reels are for connection of two potential electrodes on either sides of the stations. These connections are made with the aid of a crocodile clip on each of the electrode to make for effective contact between wires and the ground of the electrode.

(d) Hammer:

It is used to hit the electrode to the ground

(e) Global Positioning System (GPS):

This is a device that is used to determine the latitude, longitude and altitude of a particular area been surveyed.

3.2 SURVEY METHODS

Lateral variations in apparent resistivity, which reflect lateral geological variability or localised anomalous features, were investigated using an electrode array spaced consistently apart. The electrode array's size was changed in order to investigate resistance variations with depth. The Wenner-Schlumberger array configurations were used in the 2-D resistivity approach. The traverses 1 and 2 used the Wenner-Schlumberger array arrangement. The PASI resistivity metre was used in this study's implementation of 2-D resistivity methods for geophysical measurements.

A 12V, 60Ah battery, two connectors, 36 steel electrodes, crocodile-clipped connection cables, and four reels of multi-core cables are among the additional tools and accessories used.

The RES2D Inversion Software was used to understand the data. With the use of this programme, a two-dimensional (2D) "true resistivity" model of the subsurface can be created by inverting the "apparent resistivity" data from electrical imaging surveys. The programme first partitions the subsurface into many rectangular blocks, which have a weak correlation with the pseudo sections' distribution of recorded data points. The resistivity of these rectangular blocks is then calculated so as to yield an apparent resistivity pseudo section that agrees with the measured values.

For every survey line or traverse, images of the true subsurface resistivity distribution were created by inverting the apparent resistivity data. In order to accomplish this, the programme was used to create smooth model sections that would aid in geological interpretation using the apparent resistivity data. The apparent resistivity that was measured and the apparent resistivity that was produced by the computer were both represented as pseudo sections, which give skewed images of the subsurface. The intervals between the 2-D data points were 10 metres.

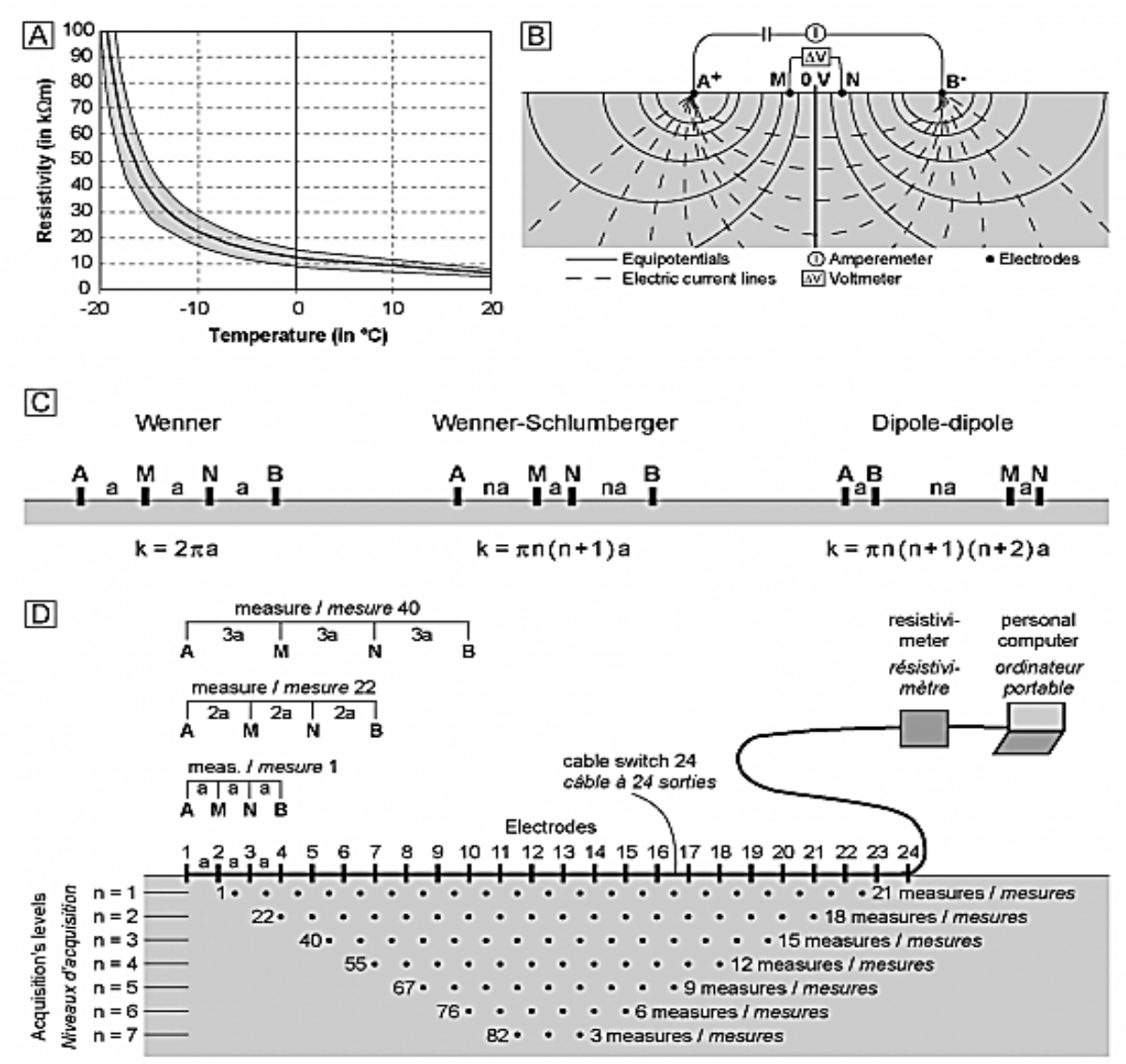

Figure 3.1: Geoelectric profiling/electrical resistivity tomography (ERT)

The electrode separation distance for each traverse ranged from $a = 10\,m$ to $a = 60\,m$ with a station interval of 10 m. The traverse length ranged from 0 – 300 m. The Wenner-Schlumberger electrode array has one current electrode (C_1) followed by two potential electrodes, (P_1 and P_2) and ends with second current electrode (C_2). For Wenner-Schlumberger, the distance between the (C_1) and (P_1) is the same as the distance between (P_2) and (C_2). The geometric factor (K) for the

Wenner-Schlumberger equals $\pi an(n+1)$. Measurements commenced at one end of the traverse line with electrode spacing $a = 10\ m$ at electrode positions 1, 2, 3 and 4. Next each electrode (C_1, P_1, P_2 and C_2) was shifted a distance of 10m, the active electrode positions being 2, 3, 4 and 5. The procedure was continued to the end of the traverse line. At each measurement, the resistivity meter displayed field resistance value and the corresponding root mean square (rms) error of the reading. The apparent resistivity of the subsurface can be computed using the formula $\pi an(n+1)R$ where "a" is the electrode spacing distance and R is the field resistance value.

3.3 DATA COLLATION AND INVERSION

Data taken from the field was entered into the computer system and computed to add the geometric factor values for each of the profile lines and saved in a text editor (notepad). The data was then read into the RES2-DINV software and then the data points checked for any bad data points. Bad data Points were exterminated but those without any had no extermination of data points. The data was then reread into RES2-DINV and inversion carried out using as many as 6 iterations. The apparent resistivity data computed for all the parallel 2-D profiles were collated to 3-D data using the RES2-DINV software. A small program was written for the RES2-DINV software in order to call the data before the collation was achieved. The collation arranged the apparent resisitivity data and the electrode layout in square grids according to the coordinates and direction of each 2-D profile used and electrodes positions in the profiles.

3.4 DATA PROCESSING

The 2-D data sets consists of a series of resistance data collected along the profiles and at different spacing and depth. The data were then arranged in an Excel sheet were each of the profile line data was multiplied with the Geometric Factors of the array that was used for the survey which gave us

the Resistivity values. A small program was written in notepad software to arrange all these data in a format that would be acceptable in Res2Dinv software for inversion.

CHAPTER FOUR

RESULTS AND DISCUSSION

4.1 RESULTS AND INTERPRETATION

In Figures 4.1 to 4.2, the 2D Electrical Resistivity models are depicted. The Inverted 2D Resistivity structures produced from the study region are provided in this model's results in a color-coded presentation. The lateral distance is scaled horizontally on the section, and the depths are scaled vertically. Both scales are in meters. All of the profiles were studied at a depth of 39 meters, with a maximum spread of 300 meters, as shown in Figures 4.1 to 4.2.

4.2 RESULTS AND INTERPRETATION

In Figures 4.1 to 4.2, the 2D Electrical Resistivity models are depicted. The Inverted 2D Resistivity structures produced from the study region are provided in this model's results in a color-coded presentation. The lateral distance is scaled horizontally on the section, and the depths are scaled vertically. Both scales are in meters. All of the profiles were studied at a depth of 58 meters, with a maximum spread of 300 meters, as shown in Figures 4.1 to 4.2.

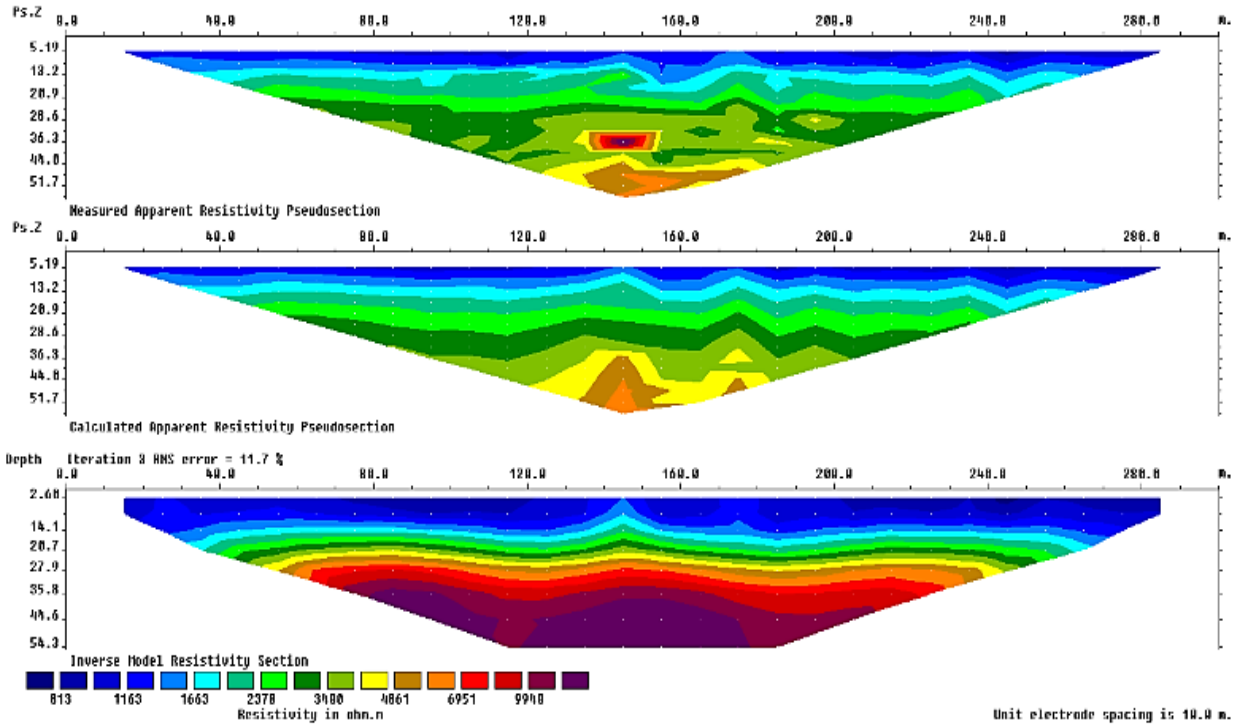

Figure 4.1: 2-D Electrical Resistivity Imaging along Traverse 1

Resistivity tomography along traverse 1 with the Wenner-Schlumberger Array uncovers varied subsurface layers, showing resistivities from 813 Ωm to 9940 Ωm: moist topsoil up to 20.7 meters (813-1163 Ωm), dry sand between 20.7 and 35.8 meters (1663-4861 Ωm), and an anomalous high-resistivity silt lens from 36.3 meters extending over 130 meters (6951-9940 Ωm), aiding in the comprehensive understanding of geotechnical properties vital for engineering decisions.

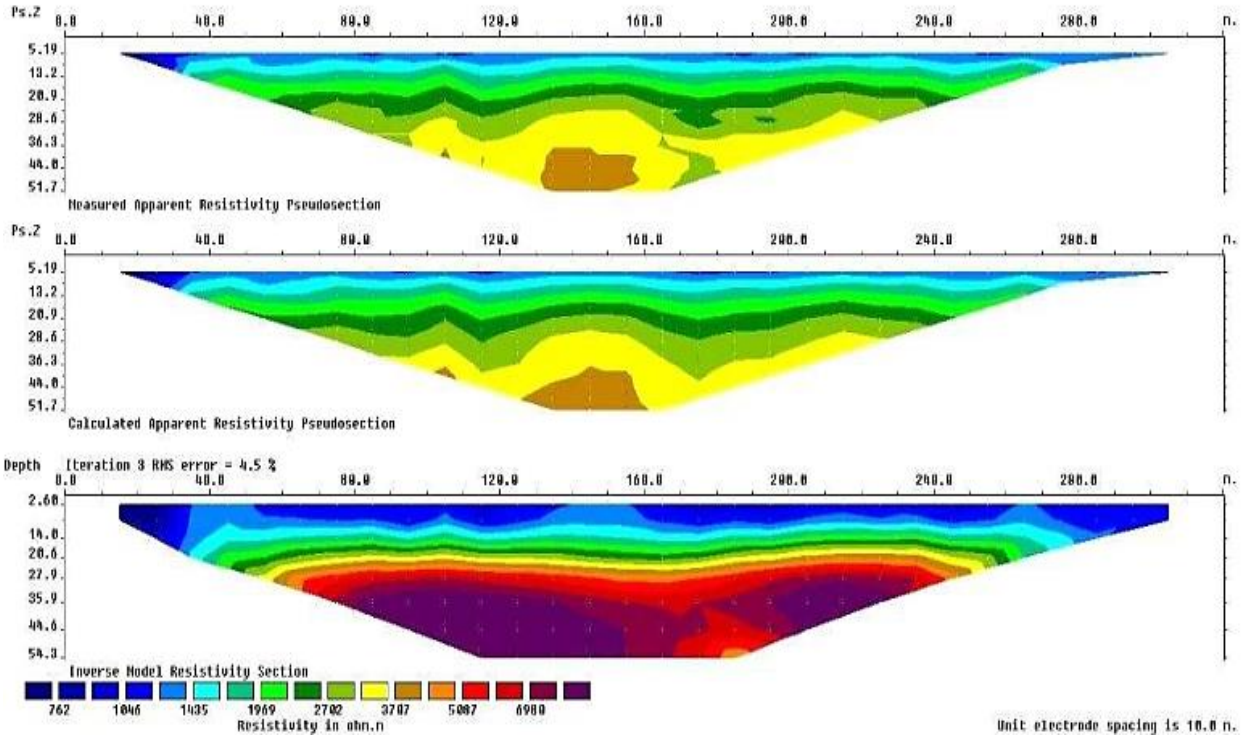

Figure 4.2: 2-D Electrical Resistivity Imaging along Traverse 2

In Figure 4.2, distinct layers with varying resistivity values indicate different subsurface materials:

Top Soil Layer: Extends from the surface to 20.6 meters depth, consisting primarily of thin topsoil with resistivity values ranging from 762 Ωm to 1046 Ωm.

Underlying Dry Sand Layer: Spans from 20.6 meters to 35.9 meters, inferred to be dry sand, with resistivity values ranging from 1435 Ωm to 3707 Ωm.

Presence of Massive Materials: From 35.9 meters to 54.3 meters, higher resistivity values (5087 Ωm to 6980 Ωm) indicate the presence of massive, less porous materials, likely fine to silty sand deposits, based on thickness and lateral extents.

CHAPTER FIVE

FINDINGS AND CONCLUSION

5.1 FINDINGS

The following are the findings from the research;

1. Traverse 1 shows moist topsoil (813–1163 Ωm) to 20.7 m, dry sand (1663–4861 Ωm) to 35.8 m, and a silt lens (6951–9940 Ωm) from 36.3 m over 130 m. Traverse 2 comprises topsoil (762–1046 Ωm) to 20.6 m, dry sand (1435–3707 Ωm) to 35.9 m, and fine/silty sand (5087–6980 Ωm) to 54.3 m.
2. The study identified three distinct subsurface layers in both traverses, with varying depths and thicknesses ranging between 20.6 to 54.3 meters**.**
3. Resistivity values align with geological formations (topsoil, dry sand, silty materials), offering insights into subsurface conditions and groundwater potential.
4. Stratigraphic mapping revealed unit extent and thickness, aiding geotechnical and groundwater studies.

5.2 CONCLUSION

This research successfully employed 2D Electrical Resistivity Imaging (ERI) to characterize the subsurface stratigraphy of Benin City, Edo State, Nigeria. Three distinct layers were delineated across the investigated traverses: topsoil, dry sand, and compact silty materials. Resistivity values ranged from 762 to 9940 Ωm, consistent with expected geological formations. ERI effectively mapped the depth, thickness, and lateral extent of these units, providing valuable insights for hydrogeological investigations, geotechnical assessments, and urban planning. By identifying potential aquifer zones and characterizing their water-bearing properties, the study demonstrates

the efficacy of ERI in groundwater exploration. Furthermore, the correlation of resistivity values with geological formations underscores the reliability of this geophysical technique for subsurface characterization in urban environments. The findings provide a robust framework for future investigations and informed decision-making in rapidly developing areas like Benin City.

REFERENCES

Abdullahi, N.K, Aboh, H.O and Masanawa, A.A (2011). Geo- electric Assessment of Groundwater potentials in Complex Basement Terrain: Case Study of College of Arts and Social Sciences, Kaduna Polytechnic Bye-Pass Campus, Northwestern Nigeria Continental J. Earth Sciences 6 (1): 1 - 7, 2011

Adebiyi, A. D., Ilugbo, S. O., Ajayi, C. A., Ojo, A. O., & Babadiya, E. G. (2018).Evaluation ofpavement instability section using integrated geophysical and geotechnical methods insedimentary terrain, Southern Nigeria. Asian Journal of Geological Research, 1(3), 1-13.

Adebo, B.A., Layade, G.O., Ilugbo, S.O., Hamzat, A.A. & Otobrise, H.K. (2019). Mapping ofSubsurface Geological Structures using Ground Magnetic and Electrical ResistivityMethods within Lead City University, SouthwesternNigeria. Kada Journal of Physics2(2), 64-73.

Aigbedion, I., Bawallah, M. A., Ilugbo, S. O., Abulu, F. O., Eguakhide, V., Afuaman, E. W., & Ukubile, B. (2019b). Geophysical Investigation for Pre-Foundation Studies at RCCG, Calvary Love Parish 2, Ukpenu, Ekpoma, Edo State, Nigeria. International Journal of Research and Innovation in Applied Science, 4(5), 39-45.

Aigbedion, I., Bawallah, M.A., Ilugbo, S.O., Abulu, F.O., Eguakhide, V., Afuaman, E.W. & Ukubile, B., (2019a). GeophysicalInvestigation for Pre-Foundation Studies at RCCG, CalvaryLove Parish 2, Ukpenu, Ekpoma, Edo State, Nigeria. International Journal of Research and Innovation in Applied Science, 4 (5), 39-45.

Aigbogun, C. O. and Egbai, J. C. (2012). Geophysical investigation of the aquiferous layers, in Uhunmwode local government area, Edo State, Nigeria. Advance in Applied Science Research, 3 (2), pp. 625-633.

Al-Fares, W. 2011. Contribution of the geophysical methods in characterizing the water leakage in Afamia B dam, Syria. Journal of Applied Geophysics. 75, 464-471.

Alile O. M. and Ehigiator M. O. (2011). Determination of the aquifer layer by the application of electrical method of exploration at Ubiaja in Edo Central of Nigeria Scientific Research and Essays, Vol. 6(2), pp. 493-498, 18

Alile, O. M. and Abraham, E. M. (2015). Three-dimensional geoelectrical imaging of the subsurface structure of university of Benin-Edo state Nigeria. Advances in Applied Science Research, 6(11), pp. 85-93

Andrews, N. D., Aning, A. A., Danuor, S. k. and Noye, R. M. (2013). Geophysical investigations at the proposed site of the KNUST teaching hospital building using 2D and 3D resistivity imaging techniques. Int. Res. Jour. Geol. Min., 3(3): 113-123.

Arjwech, R., Everett, M., Briaud, J.L., Hurlebaus, S., MedinaCetina, Z., Tucker, S. and Yosefpour, N. 2013. Electrical resistivity imaging of unknown bridge foundations. Near Surface Geophysics. 11, 591-598.

Barker, P. 1993. Techniques of archaeological excavation. Taylor and Francis e-Library.

Barker, R.D. 1997. Electrical imaging and its application in engineering investigations. Pp. 37-44, in McCann, D.M., Eddleston, M., Fenning, P.J., and Reeves, G.M., (Editors), Modern Geophysics in Engineering Geology The Geological Society, London.

Bawallah, M. A., Oyedele, A. A., Ilugbo, S.O., Ozegin, K. O., Ojo, B. T., Olutomilola, O. O.,Airewele, E. & Aigbedion, I. (2020). Evaluation of structural defects and the dynamic ofstress and strain on a building along Oluwole Area, Southwestern Nigeria, AppliedJournalof Physical Science, 2(2), 23-37.

Chambers, J.E., Ogilvy, R.D., Kuras, O., Cripps, J.C., and Meldrum, P.I., 2002. 3D electrical imaging of known targets at a controlled environmental test site. Environmental Geology, 41, 690-704.

Chambers, J.E., Wilkinson, P.B., Wardrop, D., Hameed, A., Hill, I., Jeffrey, C., Loke, M.H., Meldrum, P.I., Kuras, O., Cave, M. and Gunn, D.A. 2012. Bedrock detection beneath river terrace deposits using 3D electrical resistivity tomography. Geomorphology. 177-178, 17-25.

Dahlin, T. 2001. The development of dc resistivity imaging techniques. Computers and Geosciences. 27, 1019- 1029.

Dahlin, T. and Owen, R. (1998): Geophysical investigations of alluvial aquifers in Zimbabwe. Proceedings of the IV Meeting of the Environmental and Engineering Geophysical Society (European Section), Sept. 1998, Barcelona, Spain, 151-154.

Dahlin, T. and Zhou, B. 2004. A numerical comparison of 2D resistivity imaging with 10 electrode arrays. Geophysical Prospecting. 52, 379-398.

Ezomo, F.O (2009). "Master of Science degree Exploration Geophysics Lectures Note on Electrical and Electromagnetic Methods", Physics Department, University of Benin, Benin City, Nigeria.

Griffiths, D.H. and Barker, R.D. (1993): Two- dimensional resistivity imaging and modeling in areas of complex geology. Journal of Applied Geophysics, 29, 11-226.

Ilugbo, S.O., Adebiyi, A.D., Olaogun, S.O. & Egunjobi, T., (2018a). Application of ElectricalResistivity Method in SiteCharacterization along Ado–Afao Road, SouthwesternNigeria.Journal of Engineering Research and Reports, 1(4), 1-16.https://doi.org/10.9734/jerr/2018/v1i49871

Kearey, P. and Brooks, M. 2002. An Introduction to Geophysical Exploration, Blackwell Science Publications, U.S.A.

Kogbe, C.A. (1979): Geology of Nigeria. The Stratigraphy and Sediment of Niger Delta, Elizabethan Lagos pp 311.318.

Loke, M. H. (2001). Electrical Imaging Surveys for Environmental and Engineering Studies A Practical Guide to 2Dand 3D Surveys. www.geoelectrical.com p. 62.

Loke, M.H. 2010. 2D and 3D Electric Imaging Surveys, Geotomo Software Sdn Bsd, Malaysia.

Loke, M.H. and Lane, J.W. 2004. Inversion of data from electrical resistivity imaging surveys in water covered areas. Exploration Geophysics. 35, 266-271.

Magawata, U.Z., Gulma, M.A., Bawallah, M.A. & Ilugbo, S.O. (2020). Geotechnical Investigation of Sub-Base and Sub-Material of Kali Collapse Dam Aliero, Northwestern Nigeria, Using Laboratory Investigations. Science Journal of Advanced and Cognitive Research, 1(1), 61-75.

Marescot, L., Régis, M. and Chapellier, D. 2008. Resistivity and induced polarization surveys for slope instability studies in the Swiss Alps. Engineering Geology. 98, 18–28.

Nigerian Geological Survey Agency (2006). Geological and mineral resources map of Edo State, Nigeria, NGSA,Abuja.

Obaje, N.G. (2009). Geology and Mineral Resources of Nigeria, London: Springer DordrechtHeidelberg, 5–14.

Ogunsanwo, O. (1989). Some properties of sedimentary laterite soil as engineering construction material. International Association of Engineering Geology Bulletin, 39(1), pp. 131 135.

Okhakhu, P.A. (2014). Fundamentals of Contemporary Climatology. Ekpoma: Ambrose Alli University Press

Oyedele, A. A., Bawallah, M. A., Ozegin, K. O., Ilugbo, S. O., Ajayi, C. A. & Aigbedion, I. (2020). Probability functions of road failures in a typical basement complex region, South-western Nigeria: A case study of Akure - Oba Ile Airport Road, International Journal of Water Resources and Environmental Engineering, 12(2), 10-21. https://doi.org/10.5897/IJWREE2019.0906

Perrone, A., Lapenna, V. and Piscitelli, S. 2014. Electrical resistivity tomography technique for landslide investigation. Earth-Science Reviews. 135, 65-82.

Rucker, M. 2006. Surface geophysics as a tool for characterization existing bridge foundation and scour conditions. Proceedings of the Conference on Applied Geophysics, Missouri, U.S.A., December 4-7, 2006.

Sands TB (2002). Building stability and tree growth in swelling London clay – implication for pile foundation design. www.agu.org.